FIBER OPTIC SCANNER USING ELECTROMAGNETIC ACTUATION WITH DIFFERENT FERROMAGNETIC MATERIALS

by

PRATIBHA CHAULAGAI PHUYAL

Presented to the Faculty of the Graduate School of

The University of Texas at Arlington in Partial Fulfillment

of the Requirements

for the Degree of

MASTER OF SCIENCE IN ELECTRICAL ENGINEERING

THE UNIVERSITY OF TEXAS AT ARLINGTON

December 2006

I dedicate this thesis to my beloved husband Dilli Raj Phuyal, my daughter Deepa Phuyal, my father Prabhu Nath Chamlagai, and my mother Saraswati Chamlagai.

ACKNOWLEDGEMENTS

First of all, I would like to express my sincere gratitude to Dr. Jung-Chih Chiao, associate professor- Electrical Engineering Department at The University of Texas at Arlington for his continuous supervision, leadership, fairness and encouragement during my thesis work. This thesis work would have never been completed without his analytical inspiration. Secondly, I would like to thank my husband for his enormous support during this period who provided love and safeguard on the behalf of both parents to our daughter who was only four and half months old when I started my MS. I also would like to thank my parents who has taken care my daughter in the first half part of my MS. Equally, I would like to express gratitude to my parent in-laws Laxmi Prasad Phuyal and Chandika Devi Phuyal, who put the similar efforts to take care my daughter during the second half part of my MS study. I would like to acknowledge the support and help from ARRI, Hans Hu, Thermpon Ativanichayaphong, Smitha MN Rao, Saket Karajgikar, Narayan Paudel, and Physics Department. I would like to thank Dr. Nikolai Stelmakh and Dr. Digant Dave' for their valuable time and suggestions. Finally, I would like to thank our group, my brothers, my sisters and my friends and relatives for their moral support and suggestions.

November 20, 2006

ABSTRACT

FIBER OPTIC SCANNER USING ELECTROMAGNETIC ACTUATION WITH DIFFERENT FERRO MAGNETIC MATERIALS

Publication No. _____

Pratibha Chaulagai Phuyal, M.S.

The University of Texas at Arlington, 2006

Supervising Professor: Dr. Jung-Chih Chiao

A fiber optic scanner capable of scanning medical imaging actuated by an external magnetic field is designed and characterized using different magnetized and non magnetized ferromagnetic materials. Cobalt, Iron, Nickel, and Samarium Cobalt powders were used before and after magnetization to perform the actuation. Plastic optical fiber and a silica optical fiber are coated with 70 % enamel paint with 30 % different ferromagnetic materials mixed using brush. Due the low Young's Modulus, the plastic optical fiber could not actuate like silica optical fiber. Therefore, the silica fiber was used to conduct the experiments. The static and dynamic measurements were

preformed for the different materials before magnetization and after magnetization for different lengths 2.2cm, 3.2cm, 4.2cm, 5.2cm, 6.2cm and 7.2cm to compare their best performance. The static displacements, dynamic displacements and resonant frequencies of the scanner were measured. It is proven in this research that the length of 5.2cm and the length of 7.2cm using magnetized cobalt powder have the highest actuation statically and dynamically in terms of actuation and in terms of power consumption. The fiber optic scanner actuates 1.345 mm statistically and 1.098 mm dynamically using magnetized cobalt powder.

TABLE OF CONTENTS

Appendix

LIST OF ILLUSTRATIONS

LIST OF TABLES

CHAPTER 1

INTRODUCTION

Having smaller size and low power consumption, fiber optic devices play significant role in various industries. Applications of these devices include optical fiber communications, industrial fiber-optic sensing, biomedical imaging and sensing, and photonic signal processing. Fiber optical switches are widely used in the fields of telecommunications, optical amplitude modulator [1-3], and medical imaging [4], [5-8]. Fiber optical devices have been developed with piezoelectric [9], electrostatic [10, 11], thermal [12, 13], and electromagnetic [14-16] actuation. Since thermal devices have higher power consumption and piezoelectric and electrostatic devices require high voltage input, optical devices using electromagnetic actuation provide low power consumption and high deflection. Fiber optic scanner is based on the Optical Coherent Tomography (OCT), which is light-based imaging modality that can be used in biological systems to study tissues in vivo. OCT performs high-resolution, cross-sectional tomographic imaging of the internal microstructure in materials and biologic systems by measuring backscattered light. In vivo imaging of tissues and organs OCT uses an optical fiber to deliver low coherent broadband light source down to the very tip of a probe with scanning capability [17].

This paper explains the design and development of a low cost, flexible, simple fabrication process, low field, low power consumption, and high precision fiber optic scanner with different ferromagnetic materials using electromagnetic actuation. In the beginning of this experiment, the plastic optical fiber was used to perform the experiment. However, due to its low Young's Modulus, the scanner could not perform well. Subsequently, the fiber optic scanner was characterized statically and dynamically using silica optical fiber of lengths 2.2cm, 3.2cm, 4.2cm, 5.2cm, 6.2cm and 7.2cm. During the experiment and research process, different ferromagnetic materials such as Nickel, Cobalt, Iron, and Samarium Cobalt powders were examined before and after magnetization. The goals of this study are to find out the best ferromagnetic material among the ferromagnetic materials mentioned above for a fiber optic scanner, and to find out the best length among these lengths for a fiber optic scanner. Experimentally it is proven that the length 5.2cm and the length 7.2cm using magnetized cobalt powder have the highest actuation statically and dynamically in terms of actuation and in terms of power consumption respectively. The fiber optic scanner actuates 1.345 mm statistically and 1.098 mm dynamically using magnetized cobalt powder. Due to its high magnetic capacity, the magnetic field strength of the Samarium Cobalt powder is higher than the electromagnet used during the experiment. So, the possibility of future work using Samarium Cobalt powder is also discussed as part of the document.

CHAPTER 2

FIBER OPTIC SCANNER

2.1 Configuration of Fiber Optic Scanner

Optical fiber based scanners have been using for bar-code scanning, inspecting and vivo imaging. These devices have been playing major role in the vivo imaging in comparison to the traditional big and bulky devices. There are one dimensional, two dimensional and three dimensional scanners available. The configuration of the optical fiber based 1-D scanner is shown in Fig. 2.1. It consists of an external electromagnet, a single-mode optical fiber coated with magnetic gel, a HeNe laser, an objective lens, and a position sensitive detector (PSD). The distance between electromagnet and the magnetic coating of the fiber is kept 3mm.

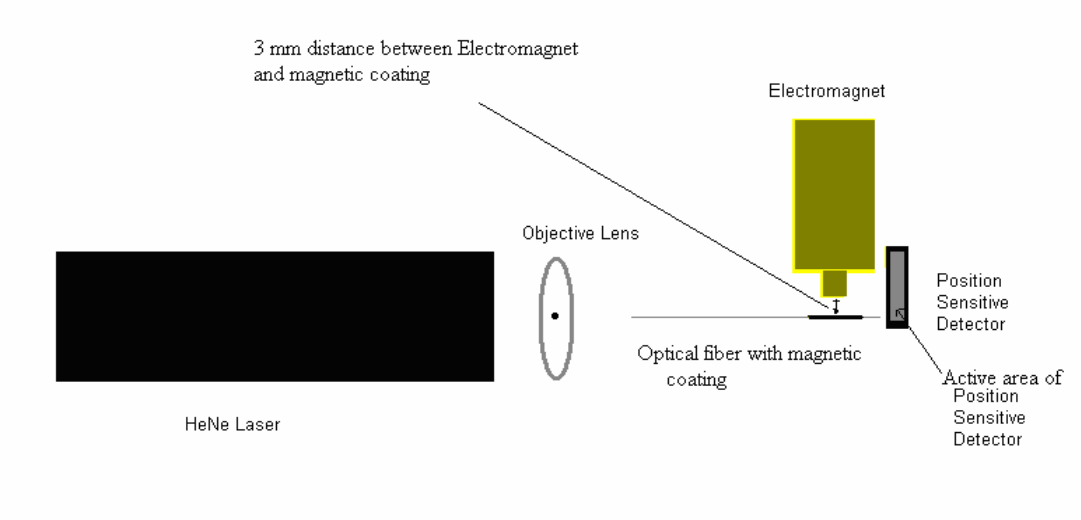

Figure 2.1: Experimental setup of the fiber optic scanner.

The HeNe laser at wavelength of 632.8 nm with optical power of 20mW laser beam focuses, onto an objective lens with focal length of about 0.5mm.The objective lens focus the laser beam to the optical fiber as shown in Fig. 2.2. So when a D.C. or an A.C. electric current applied to an electromagnet with frequencies bandwidth of 60 Hz and resistance of 30 ohm the fiber, the optical scanner starts to scan statically or dynamically.

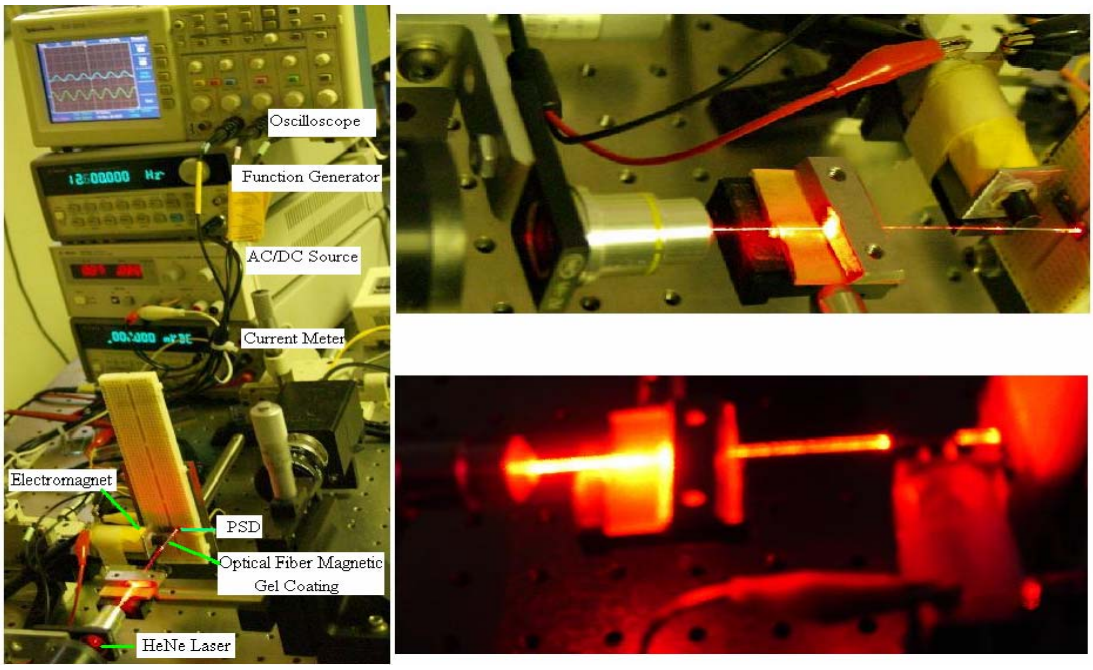

Figure 2.2: Picture of experimental setup of the fiber optic scanner.

The magnetic field strength of the electromagnet at different distance away from its magnetic core is measured experimentally by Gaussmeter (F. W. BELL 5080 Gaussmeter) [18].

A position sensitive detector (PSD) detects position data of incident spot light. It consists of a uniform resistive layer formed on one or both surfaces of a high-resistivity semiconductor substrate, pair of electrons formed on both ends of resistive layer for extracting position signal. PSD measures position, angles, distortion, vibration, and lens refraction/reflection. Linear PSD operates simply comparing two output currents, which determine the position. When a spot light strikes the active area of PSD, an electric charge proportional to the light intensity is generated at the incident position which is driven through the resistive layer and collected by the output electrodes X_1 and X_2 as photocurrents [19]. The resistance length or the active length of PSD is 12 mm. Fig. 2.3 shows the sectional view of PSD.

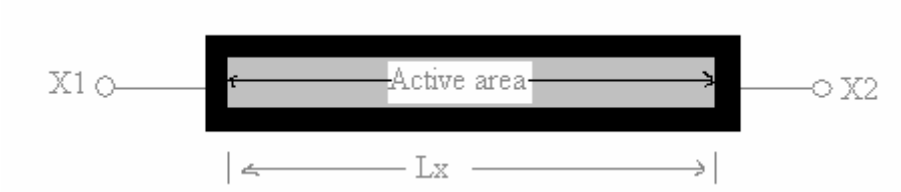

Figure 2.3: Sectional view of PSD.

The position of the incident light can be calculated by the following equation:

$$\frac{I_{X_1}}{I_{X_2}} = \frac{L_X - X}{X} \qquad (2.1.1)$$

Where,

I_{x1} = Output Current from electrode $X_{1,}$

I_{x2} = Output Current from electrode $X_{2,}$

L_x = Length of active area,

X = Distance from the electrode X_1 to the light input position.

2.2 Theory and Physical Principles

Before 1950 most permanent magnets were made from steel however in these days most high performance magnets are made from rare-earth transition-metal intermetallics such as Nd2Fe14B, and SmCo5. Due to the high permeability, low coercivity, low hysteresis loss, versatility in functions, high strength of magnetic moments, and easiness in implementation, permanent magnetic material such as NdFeB and Co-Pt have drew lots of attention in the research field [20, 21]. Magnetic materials are traditionally classified by their magnetic coercivity or hardness. Materials with low coercivity are called soft materials and those with high coercivity are called hard materials. Low coercivity material are suitable for low power and fast speed applications because the magnetic remnant flux can be removed with low reversed magnetic field [22].

The optical fiber with ferromagnetic gel coating has basically two forces. The ferromagnetic gel has magnetic force and the optical fiber itself has spring force. Due to the magnetic force the longitudinal axis of the optical fiber turns from its original position because of the bending of the fiber. This phenomenon is termed as the deflection of the fiber. Since the magnetic force induction is due to the interaction of the

magnetization of different ferromagnetic gel and the externally applied magnetic field, it can be explained as two magnets attracting each other.

2.2.1 Mechanical Analysis and Resonant Frequencies

Let's consider the Fig. 2.4, the moment-curvature for this optical fiber can be expressed as below:

$$M = EI\frac{dv^2}{dx^2} \qquad (2.2.1.1)$$

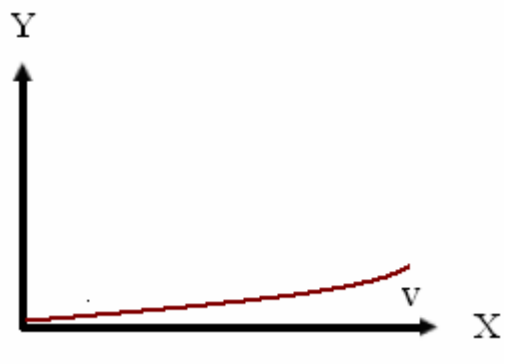

Figure 2.4: Displacements of optical fiber in y direction.

M = Bending Moment

E = Young's Modulus

I = Moment of Inertia

v = Displacements of fiber in y direction

r = radius of optical fiber

Considering an optical fiber by itself as shown in Fig. 2.5 and taking the positive bending moment at distance x. Let F_{sp} be the spring force, then the bending moment can be expressed as

$$M = - F_{sp} * x \qquad (2.2.1.2)$$

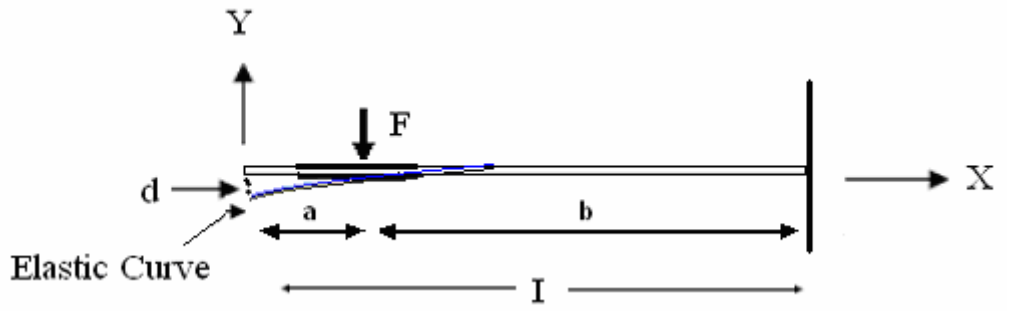

Figure 2.5: Displacements and direction of magnetic force of optical fiber.

Combining equations (2.2.1.1) and (2.2.1.2) and integrating we get

$$EI\frac{dv}{dx} = \frac{1}{2}F_{sp}x^2 + C1 \qquad (2.2.1.3)$$

At x = 1, the bending slope is equal to zero and the displacements in the y direction is zero. Integrating the equation (2.2.1.3) twice, we get

$$EI\frac{dv}{dx} = -\frac{1}{2}F_{sp}x^2 + \frac{1}{2}F_{SP}l^2 \qquad (2.2.1.4)$$

Integrating the equation (2.2.1.4) again, and when at x = 1 then the displacements in the y direction is equal to zero, the expression will be

$$Elv = -\frac{F_{sp}}{6}x^3 + \frac{1}{2}F_{sp}l^2x - \frac{1}{3}F_{SP}l^3 \qquad (2.2.1.5)$$

Therefore the bending slope and the deflection of the optical fiber at x = 0 are

$$S = \frac{F_{SP}l^3}{2EI} \qquad (2.2.1.6)$$

and

$$v = -\frac{F_{SP}l^3}{3EI} \qquad (2.2.1.7)$$

Where,

v = linear displacements of the fiber,

l = the length of the optical fiber under the bending action.

The negative sign of the deflection indicates that the deflection of fiber is downward. The spring restoring force that counteracts the magnetic force generated due to magnetic fields can be written as,

$$Fsp = \frac{3EI}{l^3}\text{v} = \text{Kv} \qquad (2.2.1.8)$$

Where K is the linear Spring Constant,

From figure 2.8 the deflection of the fiber can be calculated as,

$$d = \frac{F_{sp} b^3}{3EI} + \frac{F_{sp} a3}{2EI} \qquad (2.2.1.9)$$

Since, a + b is the total length of the fiber then the above terms are,

a = length of the fiber from the active area of the PSD to the Force

b = remaining length of the fiber

d = deflection of the fiber

$K = \frac{1}{(\frac{b^3}{3EI} + \frac{a^3}{2EI})}$ = Spring Constant

The scanner requires the minimal power to operate, at resonant frequencies. So at resonant frequencies the actuating optical fiber experiences large displacements, and oscillating motion of optical fiber are purely sinusoid. The resonant frequencies of the fiber can be calculated using Rayleigh's method [23].

$$f = \frac{1}{2\pi}\sqrt{\frac{3EI}{l^3(M + 0.23m)}} \qquad (2.2.1.10)$$

From equation (2.5.8), $K = \frac{3EI}{l^3}$ is the Spring Constant of the fiber, then the resonant frequencies can be further defined as,

$$f = \frac{1}{2\pi}\sqrt{\frac{K}{(M + 0.23m)}} \qquad (2.2.1.11)$$

Where,

f = The resonant frequencies of the fiber

M = Mass of the ferromagnetic gel

m = Mass of the optical Fiber

2.2.2 Magnetic Analysis

All magnetic moments are aligned in ferromagnetic materials because of its domains, a microscopic region.

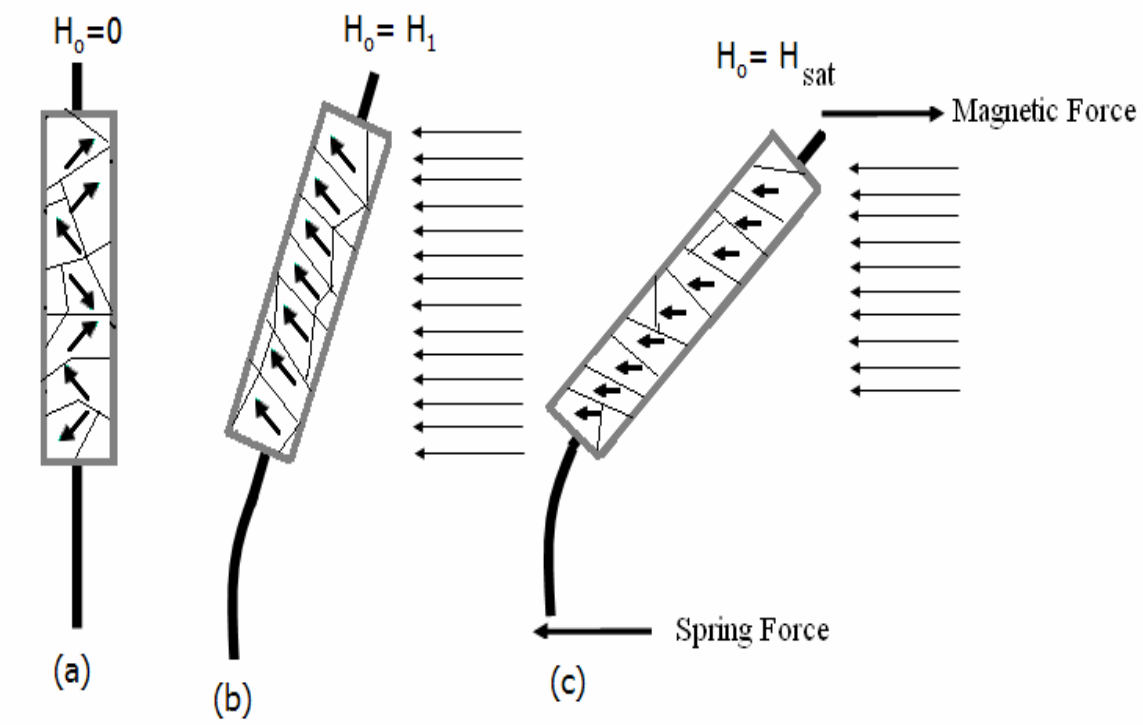

Figure 2.6: Motion of magnetic moment vectors (a) H_o=0, (b) H_o=H, and (c) H_o=$H_{sat.}$

The domains are randomly oriented in a non magnetized material which causes the net magnetic moment zero as in Fig. 2.6 (a). But if the material is placed in an external magnetic field, the magnetic moments of domains start to align with the magnetic field as in Fig. 2.6(b). The sample becomes saturated if the magnetic field is applied for long time Fig 2.6 (c).

Referring Fig. 2.7, let us consider hollow cylinder of just the ferromagnetic gel coating part and if v is the volume of that cylinder. When the magnetic field is applied to the volume v:

Poles of density, $\rho_S = \mu_{o\,M.}$

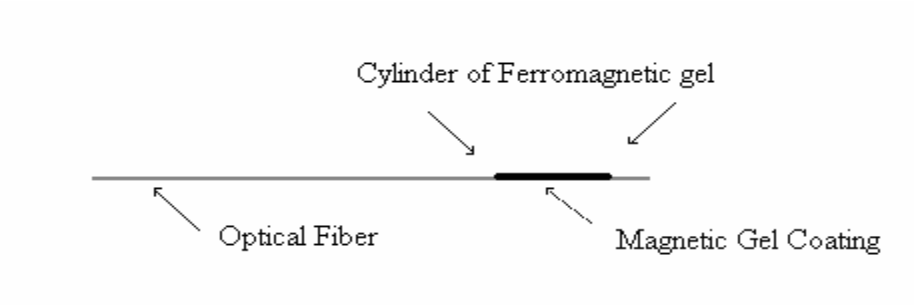

Figure 2.7: An optical fiber with magnetic gel coating.

The magnetic force can be expressed as,

$$F_{mag} = \mu_O . M . V . \frac{dH_0}{dz} \qquad (2.2.2.1)$$

2.2.3 Static Displacements

From the equations (2.2.2.1) and (2.2.1.8), the equilibrium forces can be expressed as,

$$Kd = \mu_o \text{ .M. V. } \frac{dH_0}{dz} \qquad (2.2.3.1)$$

Therefore, the static displacements of the fiber is

$$d = \mu_o \text{ .M. V. } \frac{dH_0}{dz} . \frac{1}{K} \qquad (2.2.2.2)$$

Thus, the static displacements of a material depend upon the Spring Constant and magnetic force of that material. It can be concluded that higher the value of the Spring Constant, lower the actuation and lower the value of Spring Constant higher the displacements.

2.3 Previous Fiber Optic Scanners

In the past researchers have done research on different kinds of fiber optic scanners. A three-dimensional endoscopic optical coherence tomography system based on a dual-axis scanning MEMS mirror scanner is shown in Fig. 2.8. The diameter of the MEMS mirror was 1.2 mm and both axes were capable of scanning greater than 20° with linearity [24]. But the fabrications steps of this scanner are complicated.

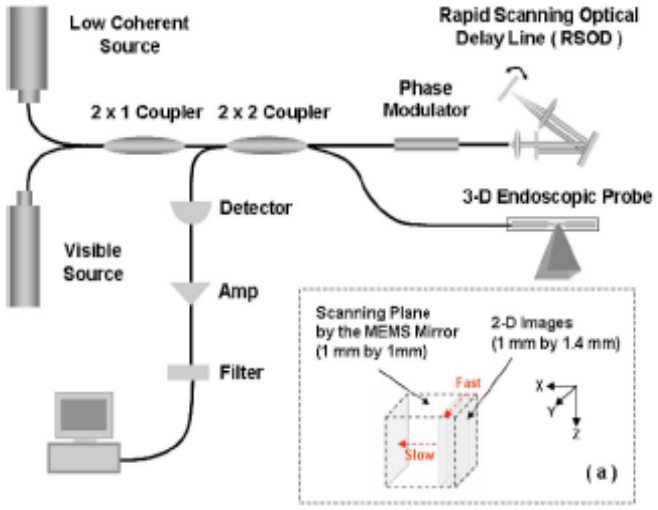

Figure 2.8: Configuration of 3-D MEMS scanner [24].

There are also two dimensional scanners can be performed either by cascading one dimensional scanner [25-27] or designing two dimensional scanners itself.

Previously 1 dimensional scanner with Nickel powder coating for lengths of silica fiber 4.2cm and 5.2cm was designed and static and dynamic characterization of the scanner was performed. The scanner was capable of 0.81 mm displacements under the influence of a static magnetic field of 17.6 KA/m in a fiber with a moveable length of 4.2cm. Dynamically, it was capable of a displacement of 0.83mm with input current amplitude of 41mA and a magnetic field of 2.4 KA/m [18].

However that scanner could not determine the best length and the best material in terms of actuation but the scanner presenting in this paper gives the alternate solution to choose the length of the fiber and to choose the ferromagnetic material itself.

2.4 Ferromagnetic Materials

Magnetism is one of the phenomena by which materials exert an attractive or repulsive force on other materials. Faraday's Law of Magnetic Induction states that when a material is placed within a magnetic field, the magnetic forces of the material's electrons will be affected. Due to the atomic and molecular structure of the material, and the net magnetic field associated with the atoms, different materials react differently to the presence of an external magnetic field. Most materials can be classified as diamagnetic, paramagnetic or ferromagnetic materials. Diamagnetic materials like copper, silver and gold have a very weak and negative susceptibility to magnetic fields and they do not retain the magnetic properties when the external field is removed. Similarly, paramagnetic materials like magnesium, molybdenum, lithium and tantalum have a small and positive susceptibility to magnetic fields and they do not retain the magnetic properties when the external field is removed.

Ferromagnetism is the normal form of magnetism and there are a number of crystalline materials that exhibit ferromagnetism. Iron, nickel, and cobalt are examples of those materials, which called the ferromagnetic materials. Most of these materials have poly-crystalline form. Samarium and neodynium in alloys with cobalt have been used to fabricate very strong rare-earth magnets. The reasons to choose the ferromagnetic materials in this experiment are ferromagnetic materials have a large and positive susceptibility to an external magnetic field, which can be permanently magnetized upon application of an external magnetic field. They exhibit a strong

attraction to magnetic fields and are able to retain their magnetic properties even after the external magnetic field has been removed. Ferromagnets can retain a memory of an applied field once it is removed. This behavior is called hysteresis and a plot of the variation of magnetization with magnetic field is called a hysteresis loop. Fig. 2.9 shows the coercivity field H_c, remnant flux M_r, and saturation flux M_s. These measurements for different ferromagnetic non magnetized and magnetized materials are majored and discussed in chapter 3 and chapter 4 respectively.

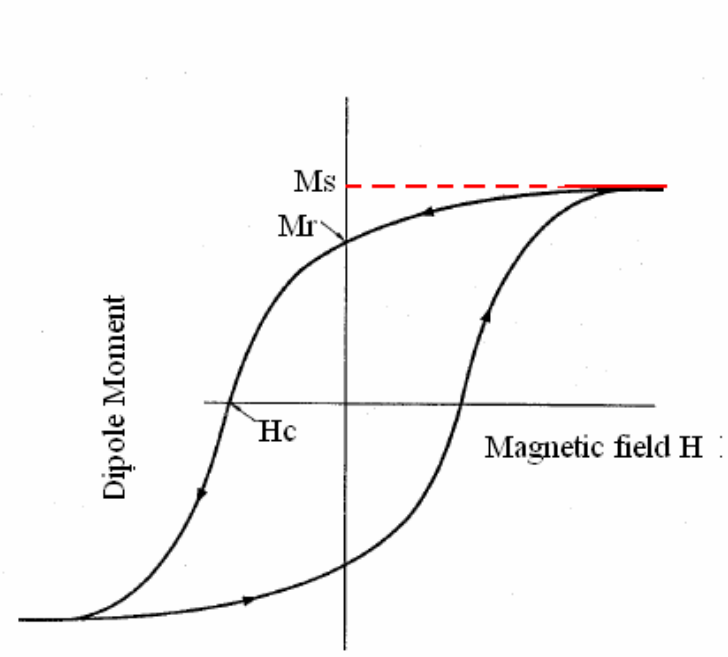

Figure 2.9: Hysteresis plot.

CHAPTER 3

FABRICATION AND RESULTS OF NON MAGNETIZED MATERIALS

3.1 Introduction

Traditionally, the fibers used to be coated using epoxy gel coating and other coating methods. In this research, the ferromagnetic materials are mixed with enamel paint and are coated using fine paint brush. In all of the experiments, 70% enamel paint and 30% ferromagnetic powder was mixed using a delicate brush. Then the optical fiber was coated in its cladding as shown in Fig 3.1.

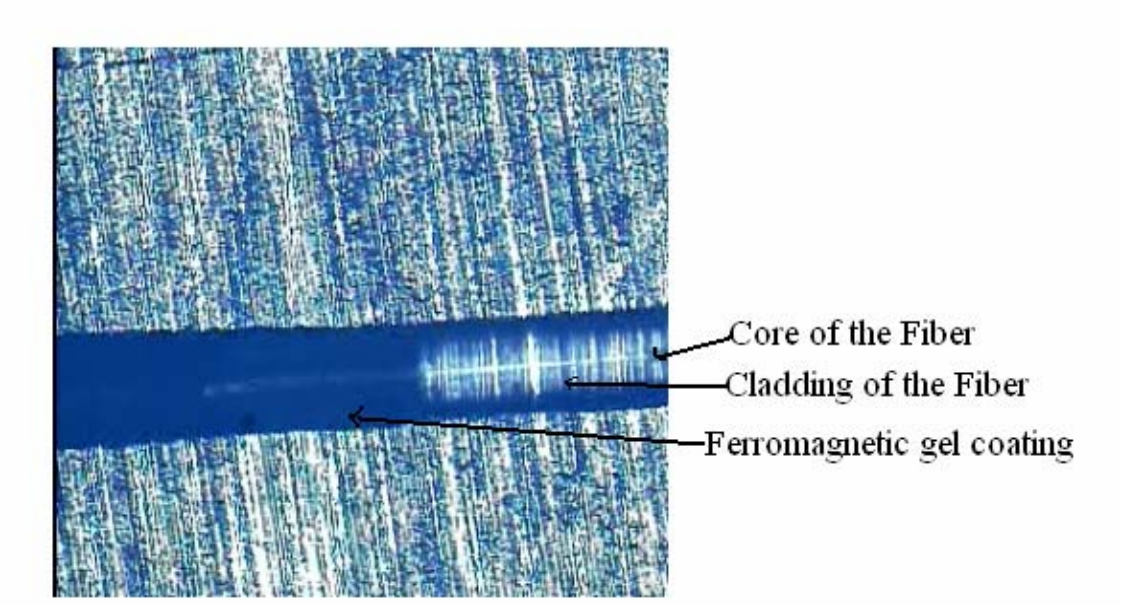

Figure 3.1: An optical fiber with magnetic gel coating.

This chapter explains the fabrication and result of a fiber optic scanner using different ferromagnetic materials using electromagnetic actuation. At first, different

material such as nickel, cobalt, samarium cobalt and iron powder were used to find out the material which gives the most actuation. Afterward, magnetized iron, magnetized cobalt and magnetized nickel are used to examine the differences between non magnetized powders and the magnetized powders. Different lengths' 7.2cm, 6.2cm, 5.2cm, 4.2cm, 3.2cm and 2.2cm of optical fibers, are used to measure the maximum deflection. Finally, the best material and the best length among those materials were chosen.

3.2 Magnetic Properties

The magnetic properties of the ferromagnetic materials are found using Alternating Gradient Magnetometer (AGM) as shown in Fig. 3.2 and MicroMag Model 2900 software. Different samples of different materials were taken in very small volume and the graph with different magnetic properties was plotted. This measurement was done with the sample in parallel with the external magnetic field in order to minimize the demagnetization effect.

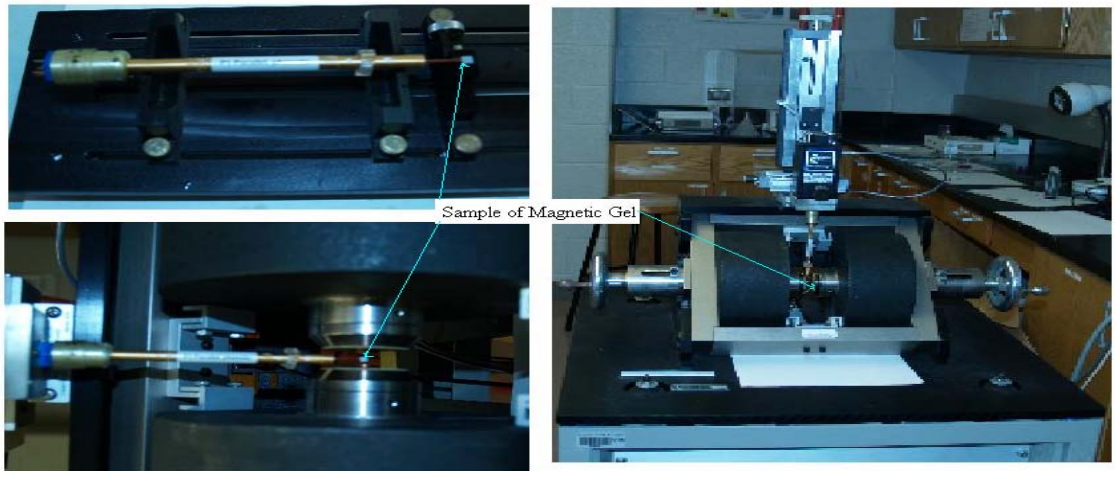

Figure 3.2: Experimental setup using AGM.

3.2.1 Nickel Powder

Magnetized and non-magnetized ferromagnetic materials were used during the experiment. The 99.99 % pure nickel powder having a particle size of 3.5 µm and density of 8.908 G/Cm^3 was used in the experiment. First of all, 30% of nickel powder was mixed with 70% enamel paint and the magnetic gel was mixed using a fine paint brush. After that the gel was prepared in a thin planar film. Then, the material was kept in air to dry for about 20 minutes and a small piece less than 3 mm in length and width of material were cut and put in the AGM to find the characteristic.

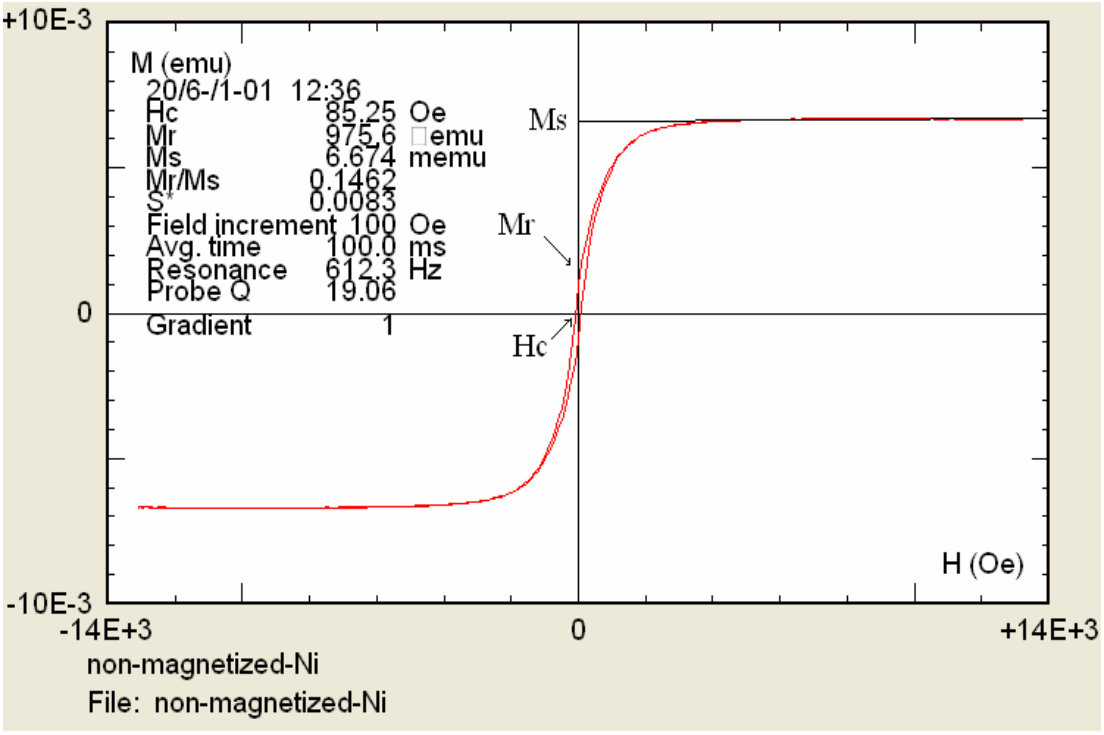

Figure 3.3: Magnetic hysterias curve for non magnetized Ni powder.

The prepared sample of Nickel powder was measured using AGM. Fig. 3.3 shows the coercivity field H_c, remnant flux M_r, and saturation flux M_s and other key parameters. The prepared sample is a planar film of 3 mm by 2 mm in area and 0.01 mm thick. This measurement was taken with the sample in parallel with the external magnetic field to minimize the demagnetization effect. The saturation magnetic volume density of the magnetic gel was found to be 33.3 KA/m.

3.2.2 Cobalt Powder

Likewise, the 99.99% pure cobalt powder having a particle size of 0.5 to 1.5 µm and density 9.92 G/Cm^3 is used in the experiment. Similar technique to the nickel coating and magnetization were used in cobalt coating.

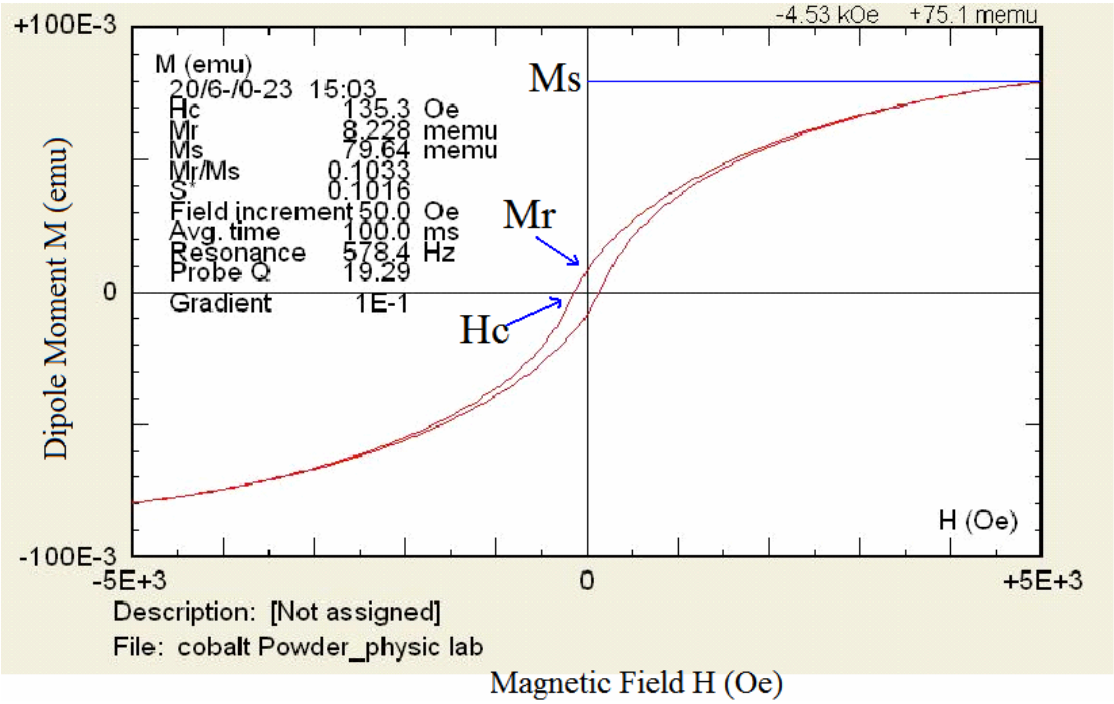

Figure 3.4: Magnetic hysterias curve for non magnetized Cobalt powder.

The coercivity field H_c, remnant flux M_r, and saturation flux M_s other key parameters for cobalt powder are shown in Fig. 3.4. The prepared sample is a planar film of 3 mm by 2.5 mm in area and 0.01 mm thick. The saturation magnetic volume density of the magnetic gel was found to be 31.8 KA/m.

3.2.3 Iron Powder

Similarly, the 99.99% pure iron powder having a particle size 44 µm and a density of 7.87 G/Cm^3 was used in the experiment. The identical techniques to the nickel coating and magnetization were used in iron coating as well.

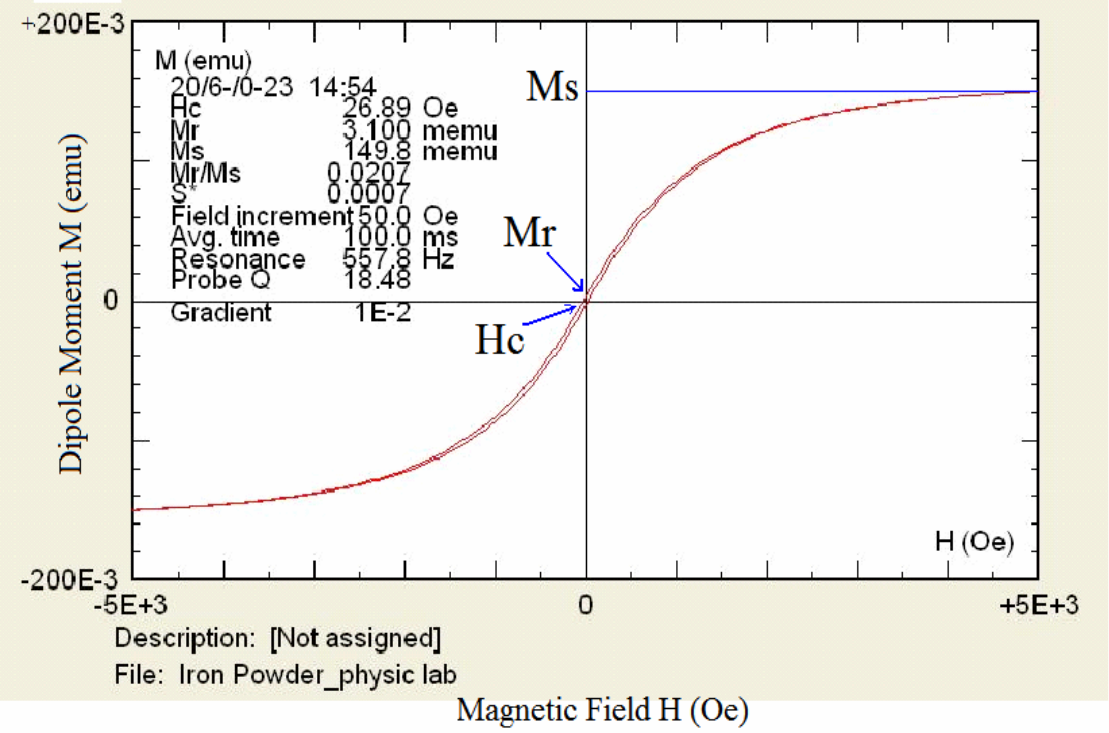

Figure 3.5: Magnetic hysterias curve for non magnetized Iron powder.

The coercivity field H_c, remnant flux M_r, and saturation flux M_s other key parameters for Iron powder are shown in Fig. 3.5. The prepared sample is a planar film of 3 mm by 2 mm in area and 0.01 mm thick. The saturation magnetic volume density of the magnetic gel was found to be 74.7 KA/m.

3.2.4 Samarium Cobalt Powder

Figure 3.6 shows the non magnetized samarium cobalt disc. The disc was broken using a piece of sand paper to make powder. The powder was mixed with paint as explained earlier.

Figure 3.6: A Samarium Cobalt disc.

Although, the coercivity field H_c, remnant flux M_r, and saturation flux M_s other key parameters for the SmCo shows in the Fig. 3.7, these are not accurate because the maximum capacity of the MicroMag is 14 kOe. Magnetic Field Strength of our electromagnet used in the experiment is 1.6×10^7 A/m, which is equal to 201 kOe. The graph of SmCo supposed to be like this graph in Fig. 2.8 but it shows way beyond the 14 kOe as shown in Fig. 3.7, which proves that our electromagnet does not have enough capacity to actuate SmCo. The prepared sample is a planar film of 2 mm by 1.5 mm in area and 0.01 mm thick. Although the saturation magnetic volume density of the

magnetic gel is shown to be 10.62 KA/m, it is not exactly correct due to the range of the AGM.

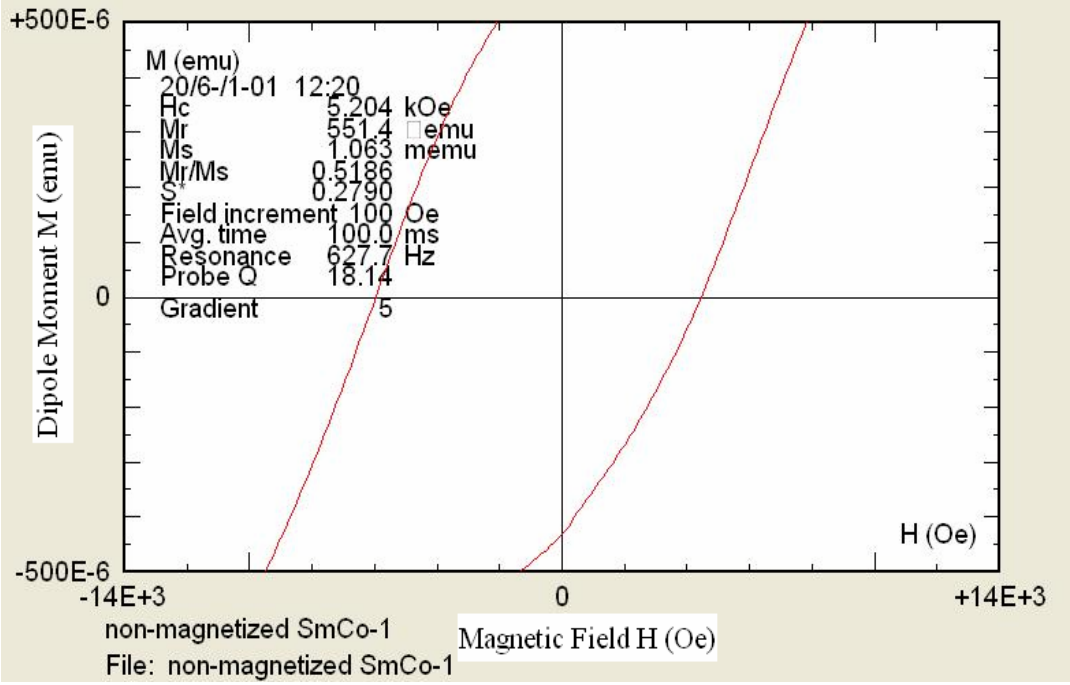

Figure 3.7: Magnetic hysterias curve for non- magnetized SmCo powder.

3.3 Actuation of Fiber using Non-Magnetized Materials

The static and dynamic measurements were performed for different lengths of fibers using non magnetized ferromagnetic materials. Iron, nickel and cobalt actuated statistically and dynamically in different input currents, but the samarium cobalt powder did not actuate statistically or dynamically at all for any length due the reason explained in the Section 3.2.4.

3.3.1 Displacements using a Plastic Optical Fiber

In the beginning of this research, the plastic optical fiber was used. Previously silica fibers of lengths 4.2cm and 5.2cm were used to do the experiment [18]. Similar lengths of 4.2cm and 5.2cm were chosen for the plastic optical fiber but the plastic optical fiber bent and the experiment could not perform. So the idea of using 2.2cm and 3.2cm fiber come to prevent the bending of the fiber having longer length. The experiment of a 2.2cm plastic fiber is done but due to the bending of fiber during the experiments the result did not satisfy the theoretical values. For static analysis, a voltage source was applied directly onto the electromagnet, and a current meter is connected in series to monitor the current flowing into the magnetic coils as shown in Fig. 3.9 in the page 28.

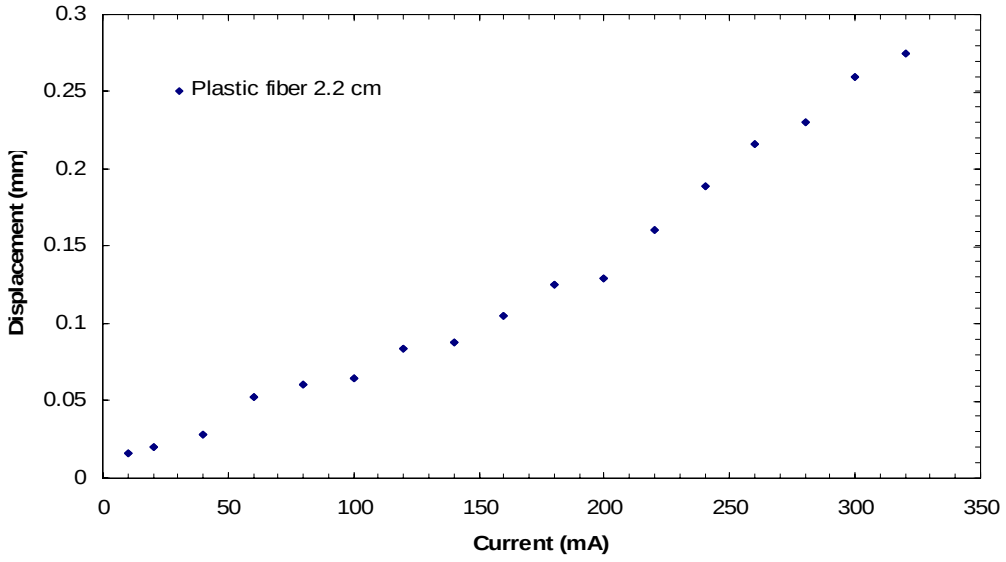

Figure 3.8: Static displacements of the 2.2cm plastic optical fiber using Ni coating.

The static measurement of the 2.2cm plastic optical fiber is shown in the Fig. 3.8. Due to the low Young's Modulus 6.7 MPa [28] of plastic optical fiber, it is not recommended for the optical scanner. Since silica optical fiber has been used in the past, has 75.39 GPa Young's Modulus and it is reliable than plastic optical fiber, we have chosen the silica optical over the plastic optical fiber. The dynamic measurement could not perform using plastic optical fiber due to its softness.

3.3.2 Static Displacements

Due to this softness of the plastic optical fiber, silica optical fiber was chosen for the experiment. To find out the static displacements of the fiber, a voltage source was applied directly onto the electromagnet, and a current meter was connected in series to monitor the current flowing. The oscilloscope was connected to monitor the voltage in PSD as shown in Fig. 3.9.

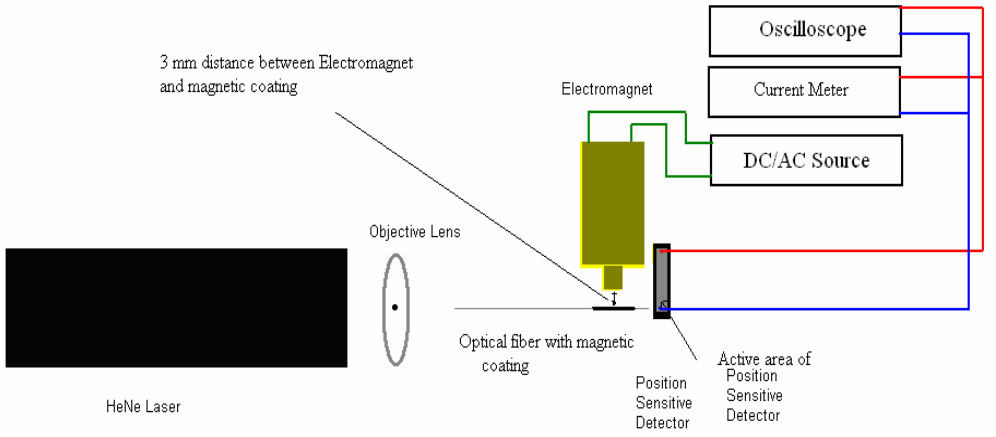

Figure 3.9: Experimental set up for static measurements.

When the end point of PSD was set as the origin, the laser light spot on the PSD screen is about 0.3 mm in diameter that gives the current output in the range of mA. The photo sensitivity at 632 nm wavelength is about 0.4 ampere per watt. Higher the length of the fiber, higher the actuation and lower the length, lower the actuation. Moreover, the thick magnetic gel coating has better actuation than the thinner coating. So the static displacements of the fiber depend upon the material, layer of coating, inputs voltage and currents, intensity of the laser beam and the length of the fiber. The actuation of the fiber due to the different lengths and different materials are explained in this section.

3.3.2.1 Length 2.2cm

The Spring Constant K for this length is $K = 244.3664 \times 10^{-3}$ N/m. Having such high spring constant, it created significant difference in the theoretical calculation. Having very low length of the fiber the fiber could not actuated in single and double coating like other lengths. In order to actuate up to this length, three layers of ferromagnetic gel were used. Further more, the theoretical static displacements and the calculated static displacements did not match. Fig. 3.10 shows the static displacements of 2.2cm silica optical fiber using Nickel coating. At first Nickel was used as ferromagnetic materials. Since the length of fiber did not support the theoretical displacements, other ferromagnetic materials were not used to do the experiment using 2.2cm length.

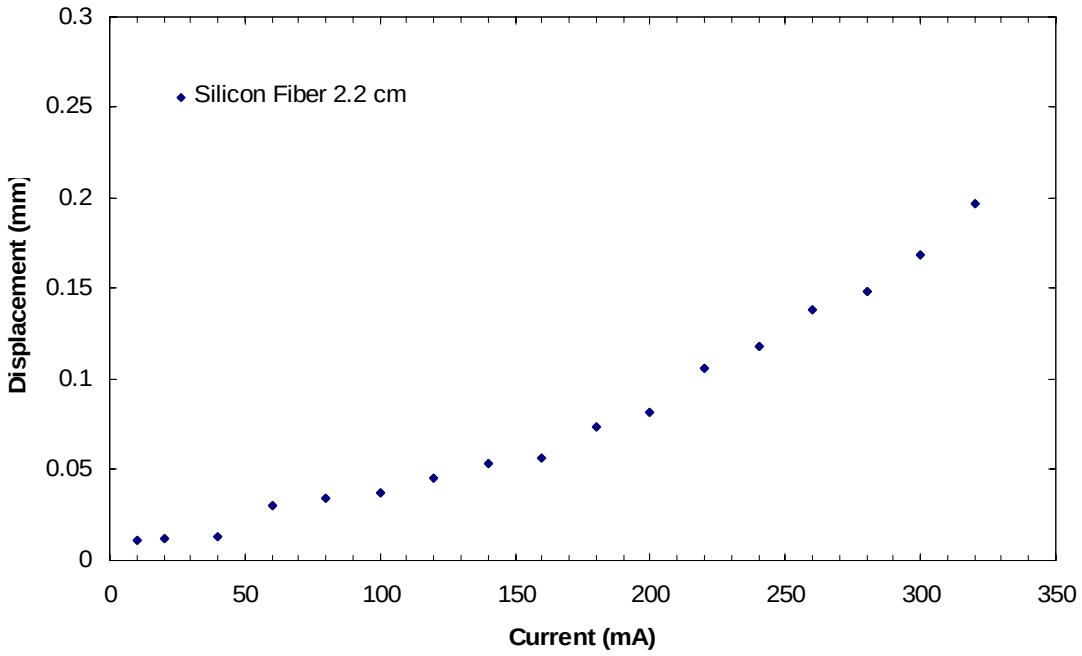

Figure 3.10: Static displacements of the 2.2cm silica optical fiber.

3.3.2.2 Length 3.2cm

The Spring Constant K for this length is K = 79.397 x 10^{-3} N/m. Likewise the length 2.2cm, due to the high spring constant, it created significant different in the theoretical calculation. Similarly this length of fiber could not actuate in single coating like other lengths but it did actuate in double coating. Similarly like 2.2cm fiber, the theoretical static displacements and the calculated static displacements did not match. Fig. 3.11 shows the static displacements of 3.2cm silica optical fiber using Nickel coating only.

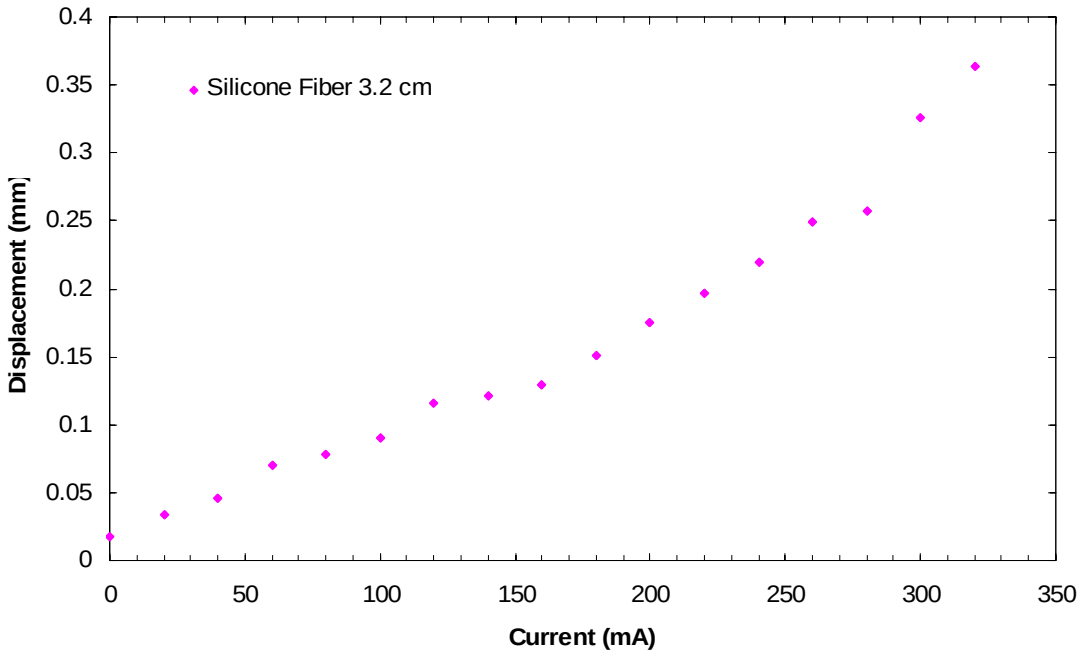

Figure 3.11: Static displacements of the 3.2cm silica optical fiber.

3.3.2.3 Length 4.2cm

The Spring Constant K for this length is K = 35.1163 x 10^{-3} N/m. Having the lower spring constant than 2.2cm and 3.2cm fiber lengths, static displacements of this length is better than previous lengths in single gel coating. Figure 3.12 shows the static displacements of 4.2cm silica optical fiber using non magnetized Nickel, Cobalt and Iron coating. It can be clearly seen in the Fig. 3.12 that Cobalt has higher actuation than Iron and Nickel. The Table 3.1 summarizes this result.

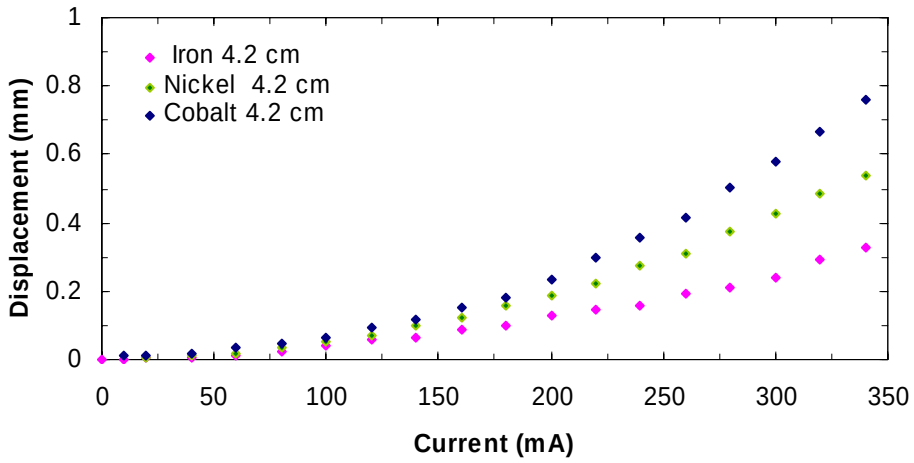

Figure 3.12: Static displacements of the 4.2cm silica optical fibers.

3.3.2.4 Length 5.2cm

The Spring Constant K for this length is K = 18.50319 x 10^{-3} N/m. The static displacements of this length are better than previous lengths. Like a 4.2cm fiber, the 5.2cm length of fiber is actuated in single coating. Figure 3.13 shows the static displacements of 5.2cm silica optical fiber using non magnetized Nickel, Cobalt and Iron coating. It can be clearly seen in the Fig. 3.13 that Cobalt has higher actuation than Iron and Nickel. The Table 3.1 summarizes this result.

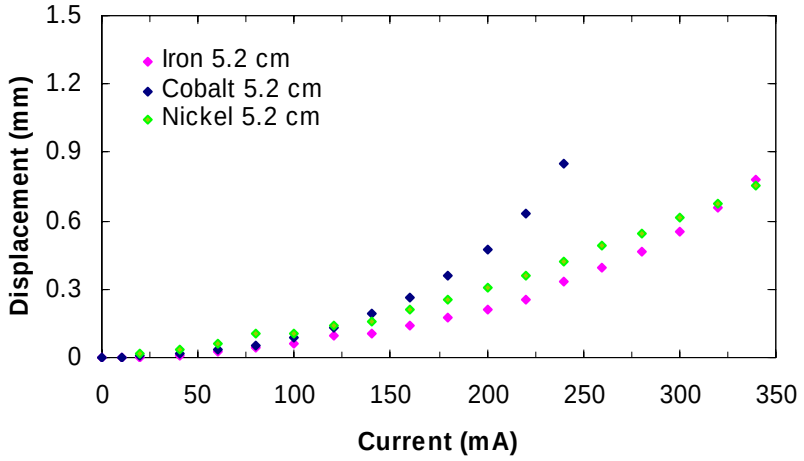

Figure 3.13: Static displacements of the 5.2cm silica optical fibers.

3.3.2.5 Length 6.2cm

The Spring Constant K for this length is K = 10.9164537 x 10^{-3} N/m. The static displacements of this length are better than previous lengths.

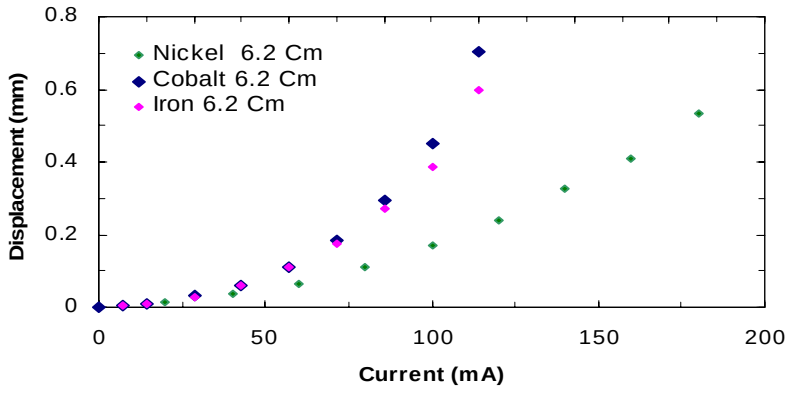

Figure 3.14: Static displacements of the 6.2cm silica optical fibers.

The 6.2cm long fiber actuated higher than 5.2cm and 4.2cm in single coating. Figure 3.14 shows the static displacements of 6.2cm silica optical fiber using non magnetized Nickel, Cobalt and Iron coating. It can be clearly seen in the Fig. 3.14 that Cobalt has higher actuation than Iron and Nickel. The table 3.1 summarizes this result.

3.3.2.6 Length 7.2cm

The Spring Constant K for this length is K = 6.9704 x 10^{-3} N/m. The theoretical and experimental static displacements of this length are better than previous lengths.

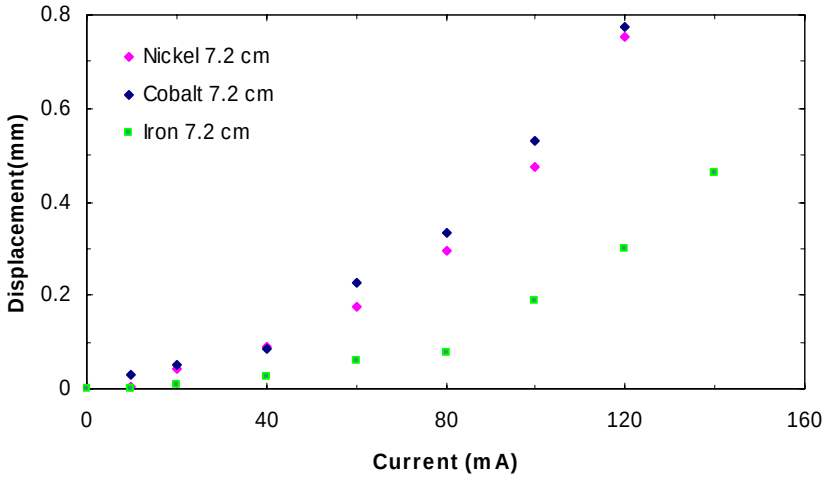

Figure 3.15: Static displacements of the 7.2cm silica optical fibers.

The 7.2cm length of fiber actuated higher than 6.2cm, 5.2cm and 4.2cm in single coating. Figure 3.15 shows the static displacements of 4.2cm silica optical fiber using non magnetized Nickel, Cobalt and Iron coating. It can be clearly seen in the Fig. 3.15 that Cobalt has higher actuation than Iron and Nickel. The table 3.1 summarizes this result.

3.3.2.7 Comparison of all Lengths for all Non Magnetized Materials

As shown in different sections above, it can be proven that the non magnetized Cobalt has the highest actuation in all length. Table 3.1 shows the displacements of fiber using different ferromagnetic materials and different lengths.

Table 3.1: Comparison of Static Displacements for Non Magnetized Materials.

Lengths (cm)	Current (mA)	Displacements using Iron Powder (mm)	Displacements using Cobalt Powder (mm)	Displacements using Nickel Powder (mm)
7.2	120	0.3003	0.7737	0.5597
6.2	160	0.3911	0.7024	0.4077
5.2	260	0.3905	0.8537	0.4889
4.2	340	0.3263	0.7605	0.5384

3.3.3 Dynamic Measurements

To perform dynamic analysis, a function generator was connected to the electromagnet and an oscilloscope was connected in series to monitor the current flowing into the magnetic coils as shown in Fig. 3.16. Due to the length itself, 2.2cm and 3.2cm fiber did not actuate like higher lengths fiber. So the experiment was done using this length by only using Nickel powder. As explained in static displacements, the

2.2cm fiber has three layer coating and the 3.2cm fiber has 2 layer coating. But 4.2cm, 5.2cm, 6.2cm and 7.2cm actuated in single coating using Iron, Nickel and Cobalt.

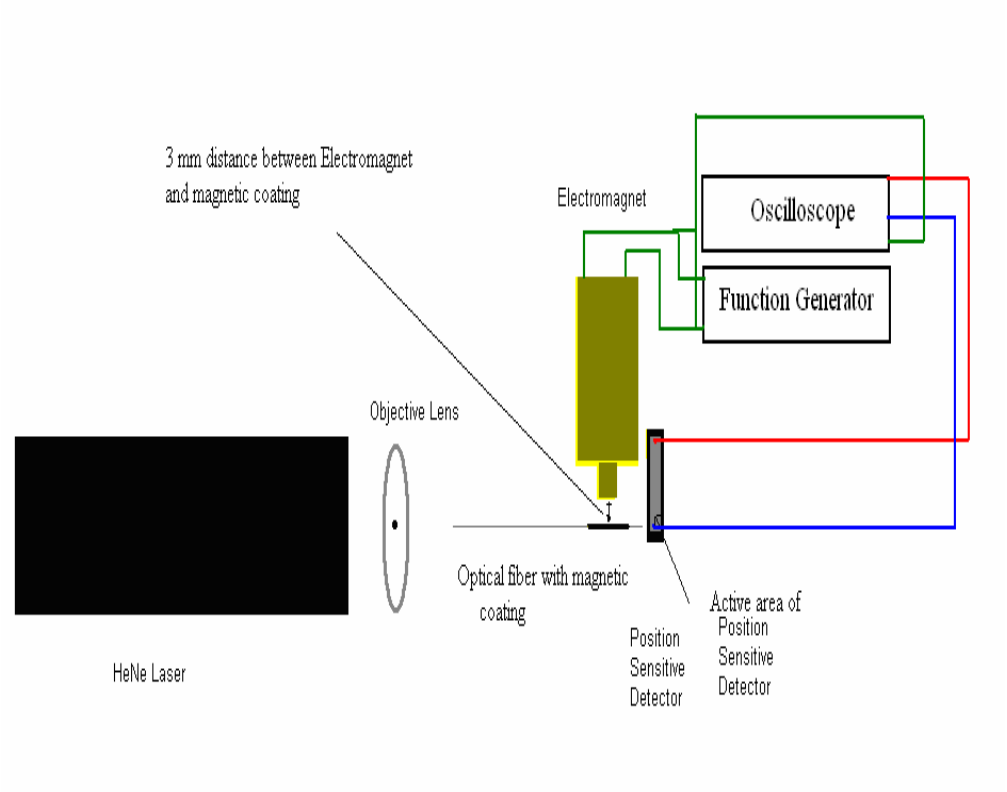

Figure 3.16: Experimental setup for dynamic measurements.

Figure 3.17 shows the input frequencies and the output frequencies. The resonant frequencies is the output frequencies of the scanner, which is approximately twice of the input frequencies. When the input frequencies is 14.3 Hz the output frequencies is 27.78 Hz for a 5.2cm non magnetized Cobalt coated fiber and when the input frequencies is 6.75 Hz then the output frequencies is 13.51 Hz for a 6.2cm non magnetized Cobalt coated fiber as shown in Fig. 3.17 .

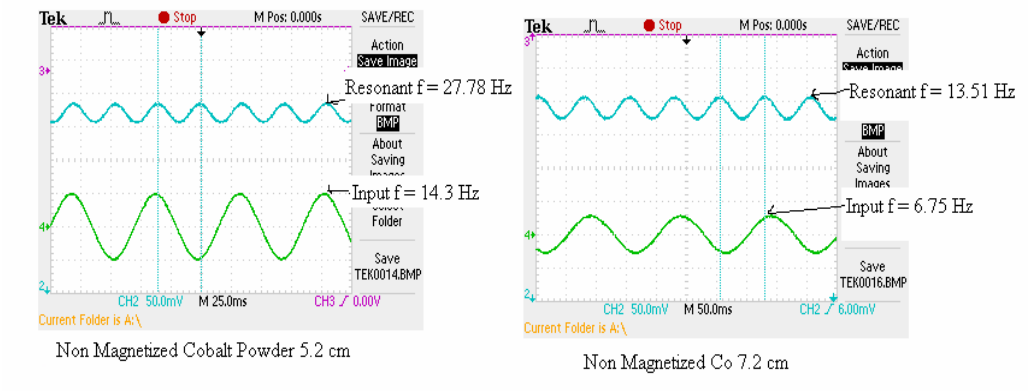

Figure 3.17: Input and output waveforms during dynamic measurements.

3.3.3.1 Nickel Powder Coating

As mentioned in the static displacements, two and three layers Nickel gel

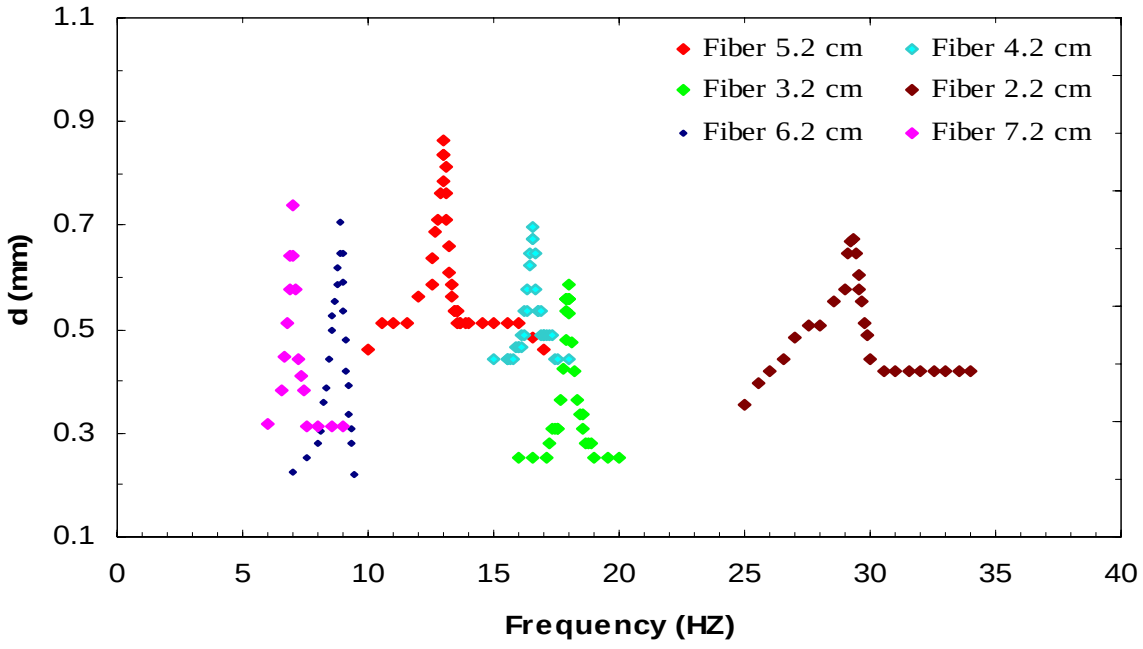

Figure 3.18: Dynamic displacements using Nickel powder coating.

were coated to perform the dynamic displacements of 3.2cm and 2.2cm fiber respectively. Only one layer of Nickel gel was coated for the other lengths of 4.2cm, 5.2cm, 6.2cm and 7.2cm. The Fig. 3.18 shows the dynamic displacements and resonant frequencies of Nickel coated fiber.

Table 3.2: Comparison of Resonant Frequencies for Nickel Coated Fibers.

Lengths (Cm)	Calculated Resonant Frequencies (Hz)	Experimental Resonant Frequencies (Hz)
2.2	68.61	59.54
3.2	44.68	52.63
4.2	31.45	33.42
5.2	24.34	26.32
6.2	17.69	18.52
7.2	13.46	13.89

Table 3.2 shows the calculated resonant frequencies for Nickel powder coating using equation (2.5.1.11). The experimental resonant frequencies show that there are some percentage errors than the calculated resonant frequencies. There could be various factors associated for this error.

3.3.3.2 Iron Powder Coating

Similarly as mentioned previous section, one layer of Iron gel was coated to perform the dynamic displacements of Iron powder using different lengths. The Fig. 3.19 illustrates the dynamic displacements and resonant frequencies of Iron powder coated fibers.

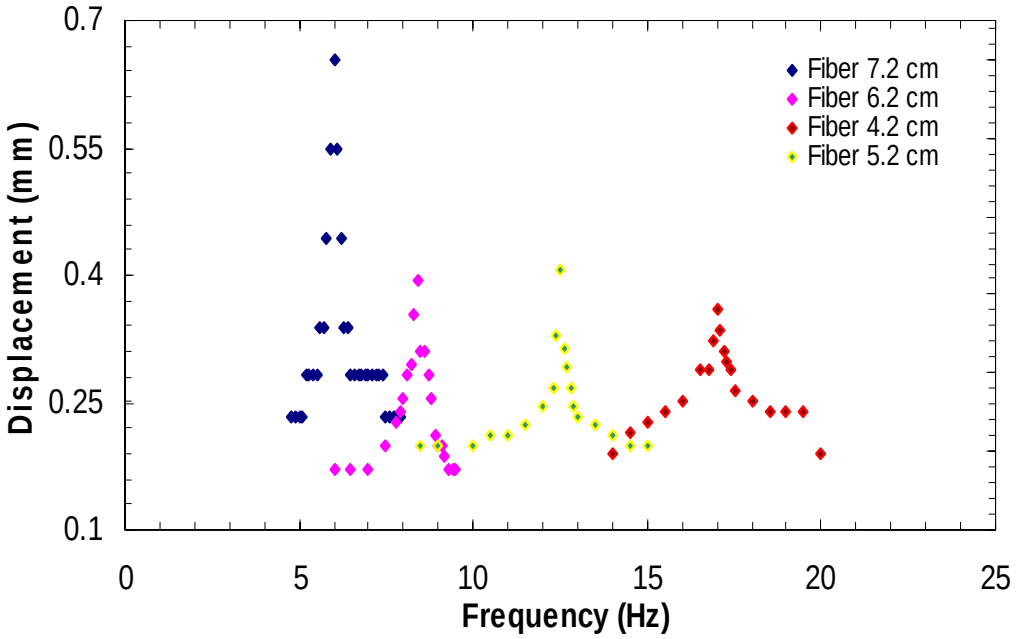

Figure 3.19: Dynamic displacements using Iron powder coating.

Table 3.3 shows the calculated resonant frequencies using equation (2.5.1.11) of the Iron Powder. The experimental resonant frequencies demonstrate that there are some percentage errors than the calculated resonant frequencies.

Table 3.3: Comparison of Resonant Frequencies for Iron Coated Fibers.

Lengths (Cm)	Calculated Resonant Frequencies (Hz)	Experimental Resonant Frequencies (Hz)
4.2	31.28	34.71
5.2	22.35	24.33
6.2	15.20	16.95
7.2	11.83	12.5

3.3.3.3 Cobalt Powder Coating

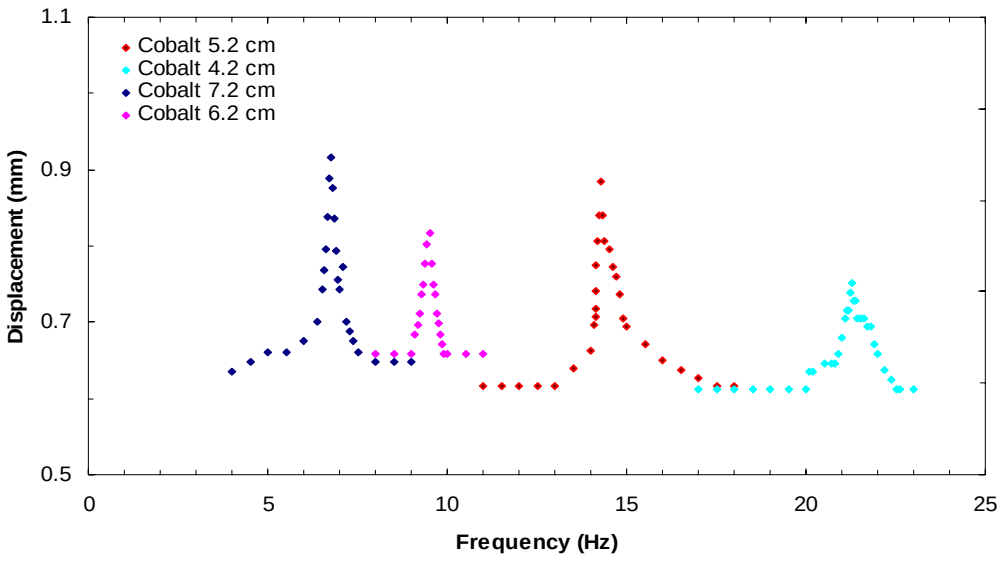

Figure 3.20: Dynamic displacements using Cobalt powder coating.

As mentioned in previous section, one layer of cobalt gel was coated to perform the dynamic displacements of Cobalt powder using different lengths. The Fig. 3.20 shows the dynamic displacements and resonant frequencies of Cobalt powder coated fibers.

Table 3.4: Comparison of Resonant Frequencies for Cobalt Coated Fibers.

Lengths (Cm)	Calculated Resonant Frequencies (Hz)	Experimental Resonant Frequencies (Hz)
4.2	37.92	40
5.2	26.75	27.78
6.2	18.23	18.52
7.2	13.21	13.51

Table 3.4 shows the calculated resonant frequencies for Cobalt powder coating using equation (2.5.1.11). The experimental resonant frequencies show that there are some percentage errors than the calculated resonant frequencies. There could be many factors for this error.

3.3.4 Comparison of the Dynamic Displacements of all Lengths

All non magnetized ferromagnetic materials have used to perform the dynamic displacements of different lengths of fibers. The table 3.5 shows that the Cobalt has the highest actuation than Nickel and Iron.

Table 3.5: Comparison of Dynamic displacements for Non Magnetized Materials.

Lengths (Cm)	Displacements using Iron Powder (mm)	Displacements using Cobalt Powder (mm)	Displacements using Nickel Powder (mm)
7.2	0.6529	0.846	0.673
6.2	0.418	0.764	0.644
5.2	0.4331	0.885	0.865
4.2	0.3875	0.751	0.697

3.4 Theoretical and Experimental Displacements of Cobalt Powder

It is proven from the experiment that non magnetized Cobalt has the highest actuation among all other materials used in this experiment. Thus, the theoretical values and experiment result for the Cobalt powder is shown in this section. The magnetization vector M was obtained by analyzing the measurement taken from AGM for the non magnetized Cobalt powder. After the data was converted to the proper unit, the polynomial equation of the magnetization vector was obtained by plotting the magnetic field strength and magnetization vector. The polynomial equation closely analyzes the magnetization vector with respect to the applied magnetic field, which is found by the curve fitting method. The unit of the magnetic field strength, magnetization vector and

the dipole moment measured from AGM is changed to SI unit using table in Appendix A.

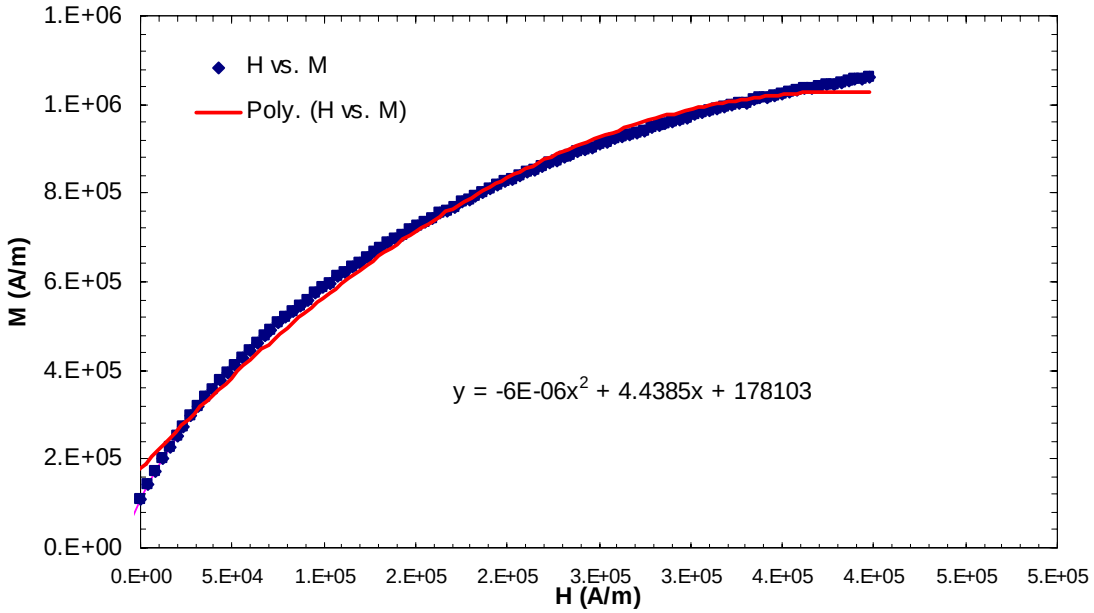

Figure 3.21: Polynomial equation of the magnetization vector.

From Fig. 3.21, it can be written,

$$M(H) = -6*10^{-06}H^2 + 4.4385H + 178103 \quad (3.4.1)$$

As mentioned earlier, the experiment was performed in the distance of 3 mm form the electromagnet to the magnetic gel of the fiber. Subsequently, the magnetization vector at 3 mm was obtained by replacing the value of x by magnetic field strength as in equation (3.4.1). Hence, the polynomial equation obtained by Fig. 3.21 was calculated using the magnetic field strength of the electromagnet, in table 3.6.

Table 3.6: Magnetic field strength of the electromagnet [18].

Input Current (mA)	H (Gauss) at 3mm	H (Gauss) at 4mm	H (Gauss) at 5mm
10	12.3	6.5	3.4
20	17.6	10	5.7
40	30	17.5	10.5
60	44.2	25.6	15.4
80	57	34.1	20.1
100	70.4	42.4	25.4
120	84.5	52	30.4
140	98.2	60.5	35.5
160	112.9	68.8	40.5
180	125	77	45.6
200	137.2	85.3	50.8
220	149.6	93.6	55.5
240	162.1	101.2	60.7
260	173.9	109.1	64.8
280	183.5	116.3	68.9
300	194.3	123.6	74
320	204	130.2	76.7
340	212	136.6	80.4
360	222	142.6	85.3

Now, we have all the parameters to calculate the theoretical static displacements using this equation (2.3.3.2). The theoretical and experimental static displacements for different lengths are shown in figures below. Due to the high value of Spring Constant K, the actuation of the 4.2cm fiber was lower than the higher lengths as in Fig. 3.22. The theoretical and experimental displacements for input current 340 mA are 0.62 mm and 0.76 mm respectively.

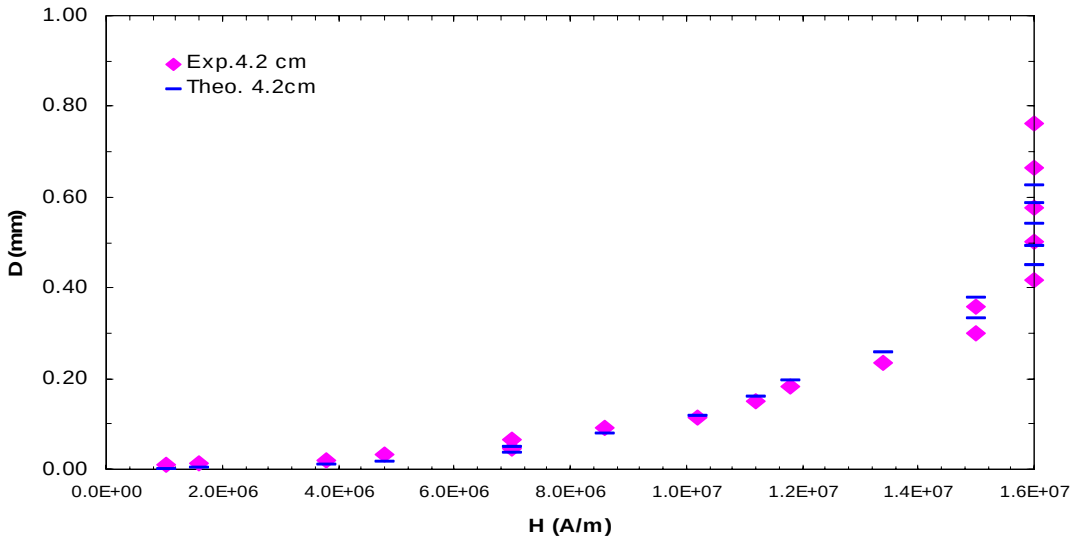

Figure 3.22: Theoretical vs. experimental static displacements of the 4.2cm fibers.

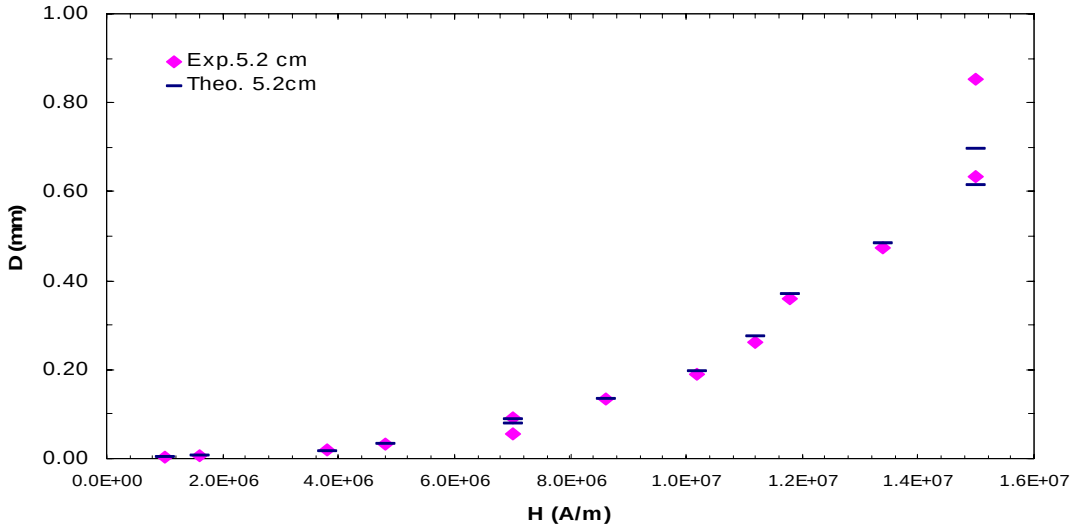

Figure 3.23: Theoretical vs. experimental static displacements of the 5.2cm fibers.

The actuation of the 5.2cm fiber is shown in Fig. 3.23. The theoretical and experimental displacements for input current 260 mA are 0.79 mm and 1.29 mm respectively.

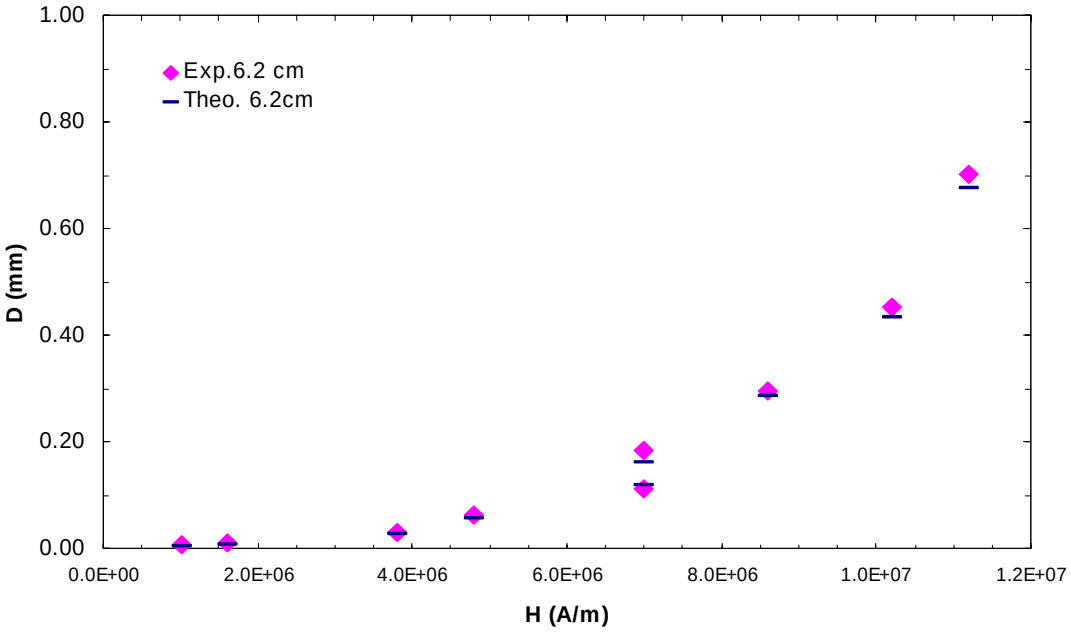

Figure 3.24: Theoretical vs. experimental static displacements of the 6.2cm fibers.

Figure 3.24 shows the displacements of 6.2cm fiber. Having low spring constant, this Fiber actuates more than lower lengths fiber, the theoretical and experimental displacements for input current 160 mA are 0.51 mm and 0.70 mm respectively. However the length 7.2cm fiber has the highest displacements than any other lengths under the same input current. For the 120 mA input current for 7.2cm fiber the theoretical and the experimental displacements are 0.56 mm, and 0.77 mm respectively.

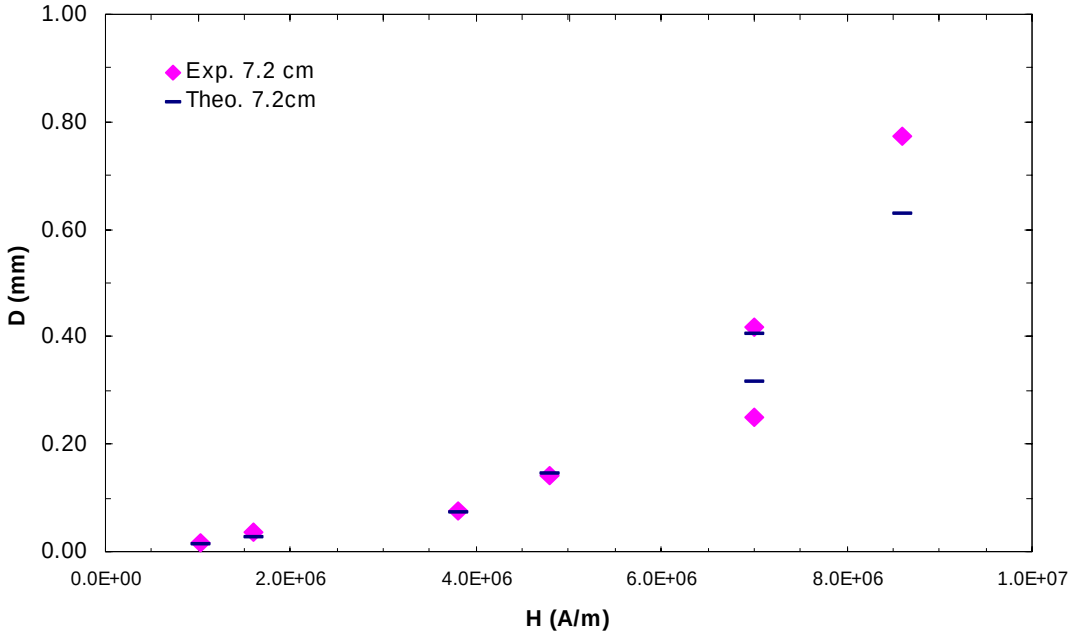

Figure 3.25: Theoretical vs. experimental static displacements of the 7.2cm fibers.

3.5 Conclusions

In brief, magnetic characteristics of the ferromagnetic materials were measured using MicroMag. The magnetic hysrersis curve and the other magnetic properties are found different for different ferromagnetic materials. The different non magnetized ferromagnetic materials were tested for fiber optic scanner. Among the non magnetized materials, Cobalt has the highest displacements comparing to Nickel and Iron. The length 5.2 has the highest displacements among other 7.2cm, 6.2cm 4.2cm while the input current is 260 mA. But in the point of view of powder consumption, 7.2cm fiber has the highest displacements among lengths 2.2cm, 3.2cm, 4.2cm, 5.2cm and 6.2cm

while the input current is 120 mA. The electromagnet used during the experiment has only 201 kOe magnetic field intensity but the Samarium Cobalt powder has higher magnetic field intensity than the electromagnet. Thus, the actuation of the non magnetized SmCo is negligible due to the weak electromagnet.

CHAPTER 4

FABRICATION AND RESULTS OF MAGNETIZED MATERIALS

4.1 Introduction

In order to observe the differences between the magnetized and non magnetized ferromagnetic materials, Iron, Cobalt, Nickel and Samarium Cobalt powders were magnetized. At the beginning, the magnetization was done in simple and traditional way. For magnetization process, a permanent magnet was placed in the top of the ferromagnetic gel coated fiber for a week. After placing the magnet successfully for a week, the coated gel was magnetized. For the fabrication, similar procedure as explained in chapter three was followed.

4.2 Magnetization

The magnetic properties of the magnetized ferromagnetic materials had been characterized like in chapter three. The hysteresis loop of the different magnetized ferromagnetic materials can be seen in following sections. Finally the magnetization is done by putting the fiber with permanent magnet for a week. To do the magnetization, some of the coated fibers are wrapped inside a paper and magnet and were put on the top of the paper so that the nickel particle would not separate from the fiber due to the polarization effect. Similarly, as explained in chapter three, it was placed with permanent magnet for a week to measure the key magnetic parameters.

The coercivity field H_c, remnant flux M_r, and saturation flux M_s other key parameters for Magnetized Nickel powder are shown in Fig. 4.1. The prepared sample is a planar film of 2 mm by 2.5 mm in area and 0.01 mm thick. The saturation magnetic volume density of the magnetic gel was found to be 90.9 KA/m.

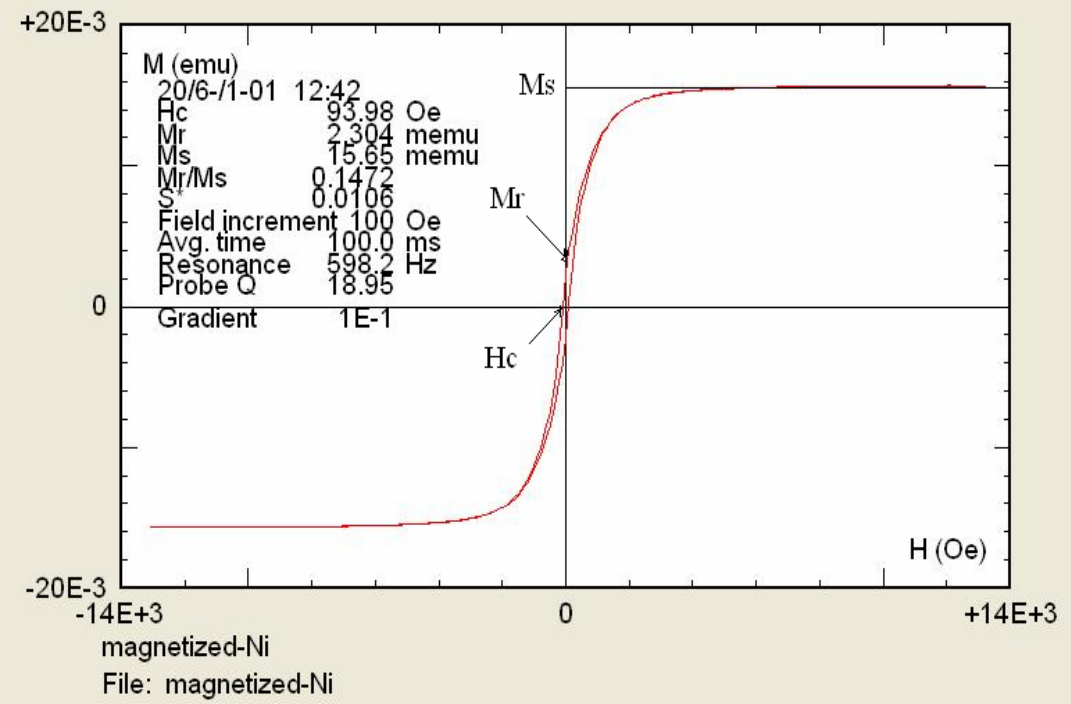

Figure 4.1: Magnetic hysterias curve for magnetized Ni powder.

The coercivity field H_c, remnant flux M_r, and saturation flux M_s other key parameters for magnetized Iron powder are shown in Fig 4.2. The prepared sample is a planar film of 2 mm by 2 mm in area and 0.01 mm thick. The saturation magnetic volume density of the magnetic gel was found to be 194.1 KA/m.

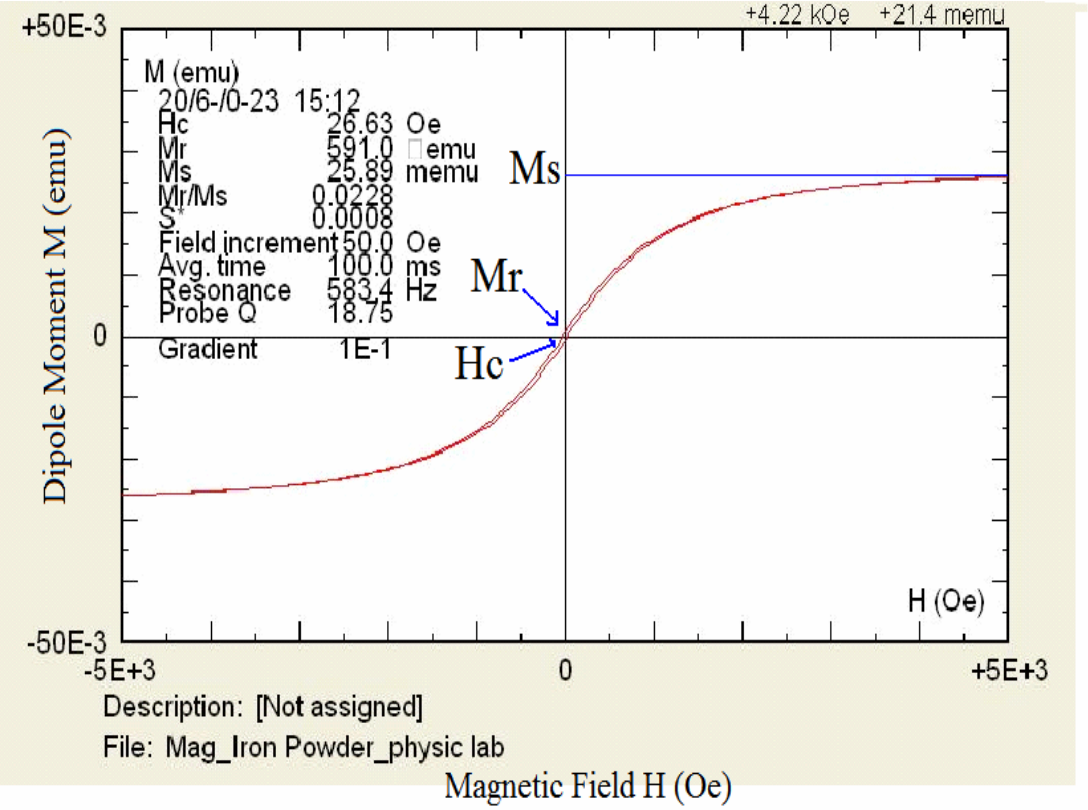

Figure 4.2: Magnetic hysterias curve for magnetized Iron powder.

The coercivity field H_c, remnant flux M_r, and saturation flux M_s other key parameters for magnetized Cobalt powder are shown in Fig. 4.3. The prepared sample is a planar film of 3 mm by 2.5 mm in area and 0.01 mm thick. The saturation magnetic volume density of the magnetic gel was found to be 31.5 KA/m.

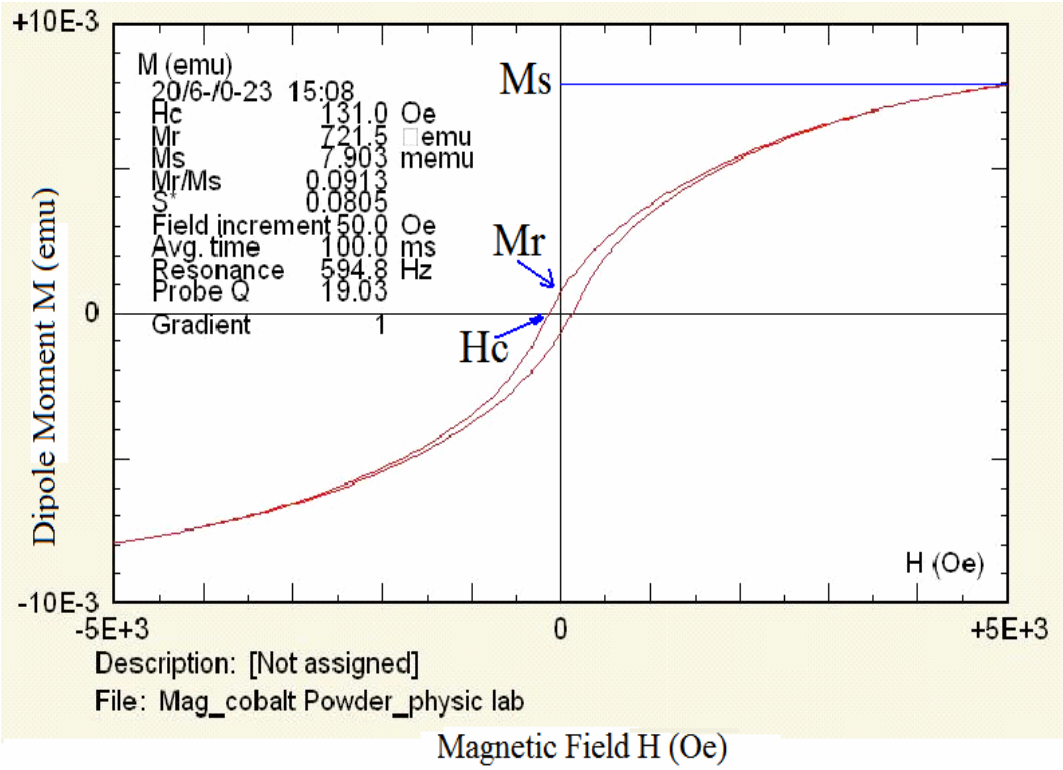

Figure 4.3: Magnetic hysterias curve for magnetized Cobalt powder.

As explained in section 3.2.4, the coercivity field H_c, remnant flux M_r, and saturation flux M_s other key parameters for the SmCo shown in figure 4.4 are not accurate. The Fig. 4.4 is the compress figure for the magnetized SmCo, the real figure of this material is like non magnetized SmCo. That's why there is negligible actuation of the magnetized SmCo only of length 7.2cm. The prepared sample is a planar film of 3 mm by 1.2 mm in area and 0.01 mm thick. Although the saturation magnetic volume density of the magnetic gel is shown to be 19.59 KA/m, it is not right due to the range of the AGM.

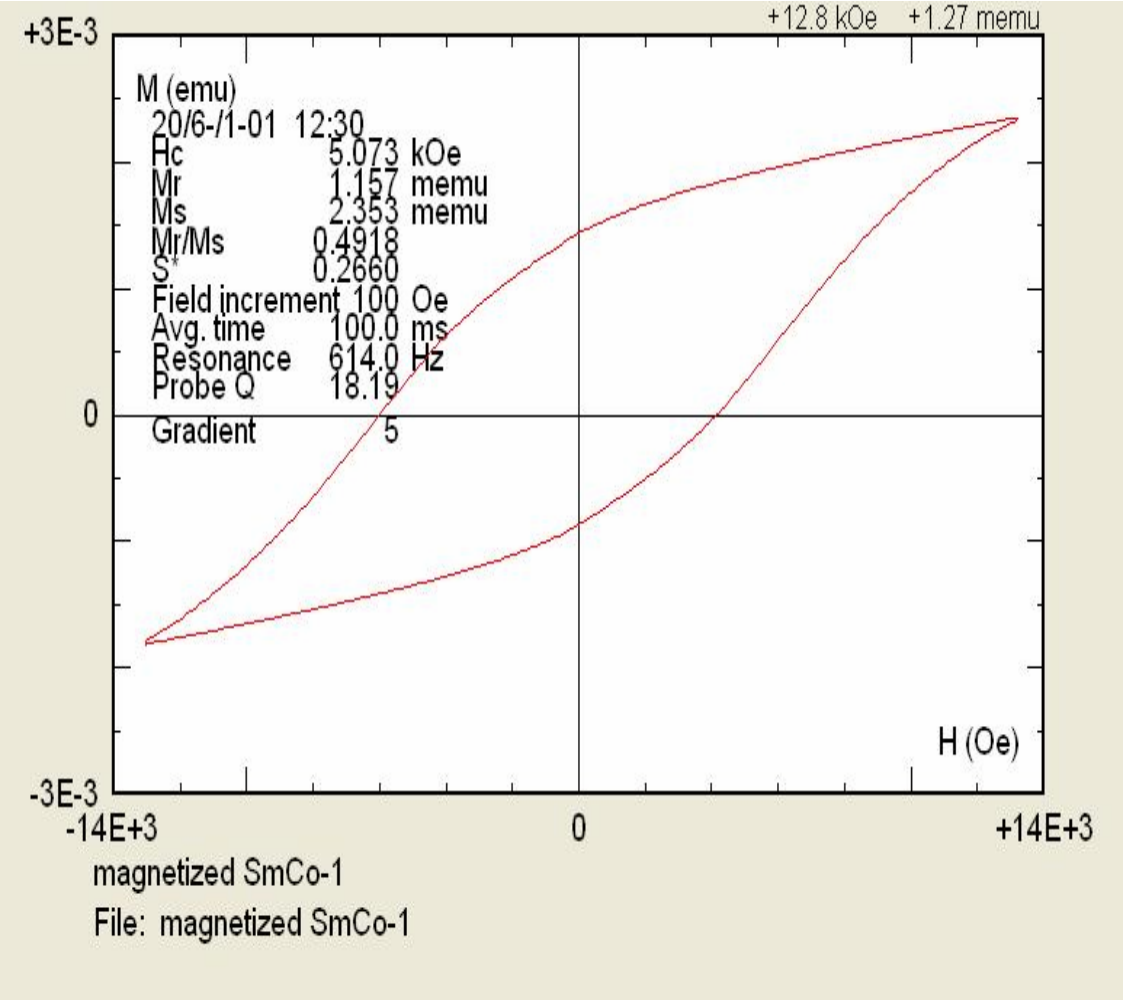

Figure 4.4: Magnetic hysterias curve for magnetized SmCo powder.

Table 4.1 shows the magnetic properties of the ferromagnetic materials varies before the magnetization and after the magnetization. There is not much different on coercivity field but there is significant difference in remnant flux and saturation flux between magnetized and non magnetized materials of the same magnetic gel.

Table 4.1: Magnetic Properties of Materials Before and After Magnetization.

Materials	Coercivity field Hc (Oe)	Remnant flux Mr (memu)	Saturation flux Ms (memu)
Iron	26.89	3.1	149.8
Magnetized Iron	26.63	591	25.89
Cobalt	135.3	8.228	79.64
Magnetized Cobalt	131	721.5	7.903
Nickel	85.25	975.6	6.674
Magnetized Nickel	93.98	2304	15.65
Magnetized and non-magnetized SmCo	Out of range of AGM	Out of range of AGM	Out of range of AGM

4.3 Static Displacements of Magnetized Materials

The static measurement of magnetized ferromagnetic materials is done similar procedure explained in chapter 3. Magnetized materials have better actuation than non magnetized materials under the same input currents and other same conditions for all lengths and materials. The theoretical and the experimental graphs of different lengths are presented in this section. The magnetized materials actuate more than the non magnetized materials in low input current.

4.3.1 Length 4.2cm

The static displacements using different magnetized ferromagnetic materials for

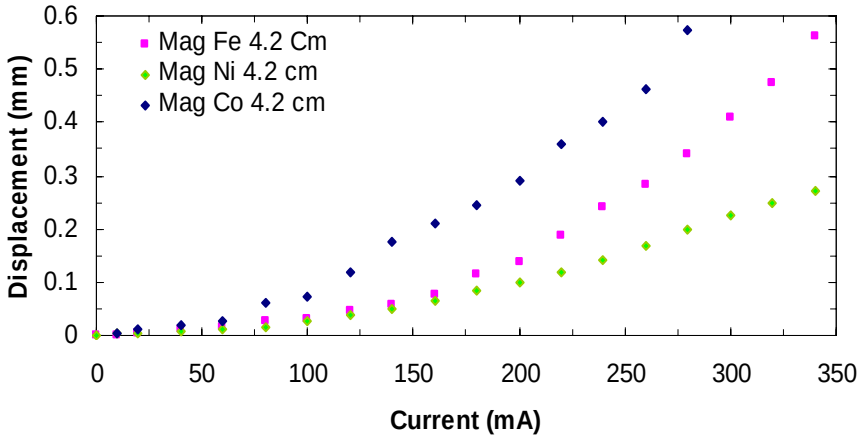

Figure 4.5: Static displacements of the 4.2cm silica optical fibers.

4.2cm length is shown in Fig. 4.5. The figure shows that magnetized Cobalt has the higher actuation than magnetized Nickel and magnetized Iron. Table 4.2 summarizes the result of it.

4.3.2 Length 5.2cm

The static displacements using different magnetized ferromagnetic materials for 5.2cm length is shown in Fig. 4.6. The figure shows that magnetized Cobalt has the higher actuation than magnetized Nickel and magnetized Iron. Table 4.2 summarizes the result of it.

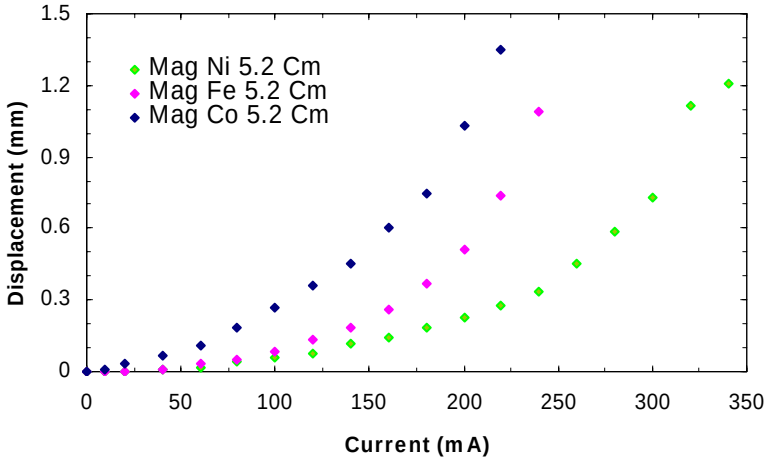

Figure 4.6: Static displacements of the 5.2cm silica optical fibers.

4.3.3 Length 6.2cm

The static displacements using different magnetized ferromagnetic materials for 6.2cm length is shown in Fig. 4.7. The figure shows that magnetized Cobalt has the higher actuation than magnetized Nickel and magnetized Iron. Table 4.2 summarizes the result of it.

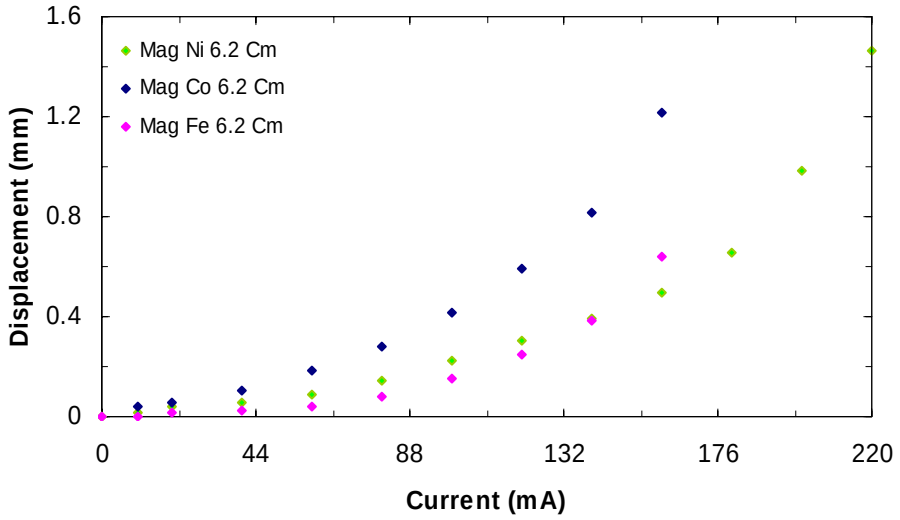

Figure 4.7: Static displacements of the 6.2cm silica optical fibers.

4.3.4 Length 7.2cm

The static displacements using different magnetized ferromagnetic materials for 7.2cm length is shown in Fig. 4.8. The figure shows that magnetized Cobalt has the higher actuation than magnetized Nickel and magnetized Iron. Table 4.2 summarizes the result of it.

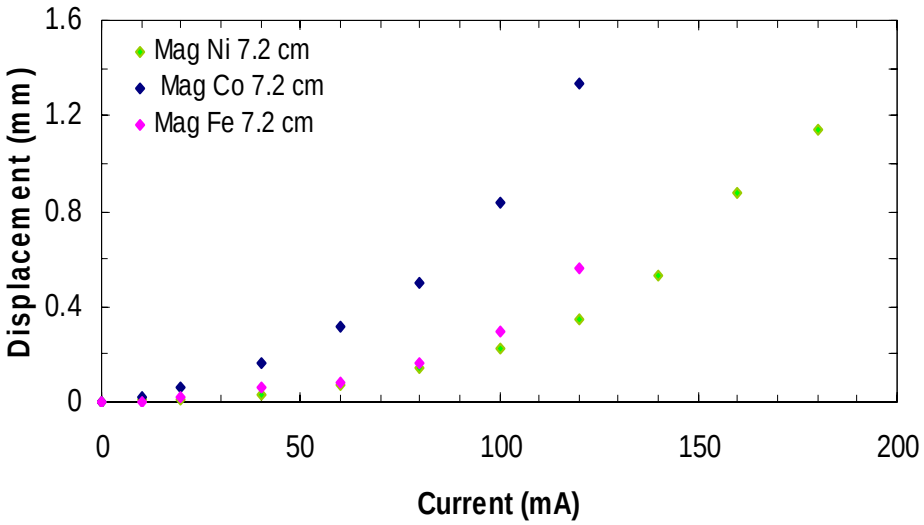

Figure 4.8: Static displacements of the 7.2cm silica optical fibers.

4.3.5 Comparison of Static Displacements for Magnetized Materials

The results from the above sections prove that the non magnetized Cobalt has the highest actuation than all the other ferromagnetic materials for all lengths used during the experiment. Table 4.2 shows the displacements of fiber using different ferromagnetic materials and different lengths. Iron actuated more than Nickel in all lengths. If we compare the same material in terms of length, length 5.2cm has the highest actuation than all other lengths.

Table 4.2: Comparison of Static Displacements for Magnetized Materials.

Lengths (Cm)	Current (mA)	Displacements using Iron Powder (mm)	Displacements using Cobalt Powder (mm)	Displacements using Nickel Powder (mm)
7.2	120	0.5616	1.337	0.3418
6.2	160	0.6393	1.212	0.4991
5.2	220	0.7342	1.345	0.2726
4.2	340	0.5616	0.8424	0.2719

4.4 Dynamic Measurements

The dynamic measurements for different materials and lengths are preformed on the same ways as explained in chapter 3. The output waveforms of magnetized cobalt powder length 5.2cm and 6.2cm is shown in Fig. 4.9.

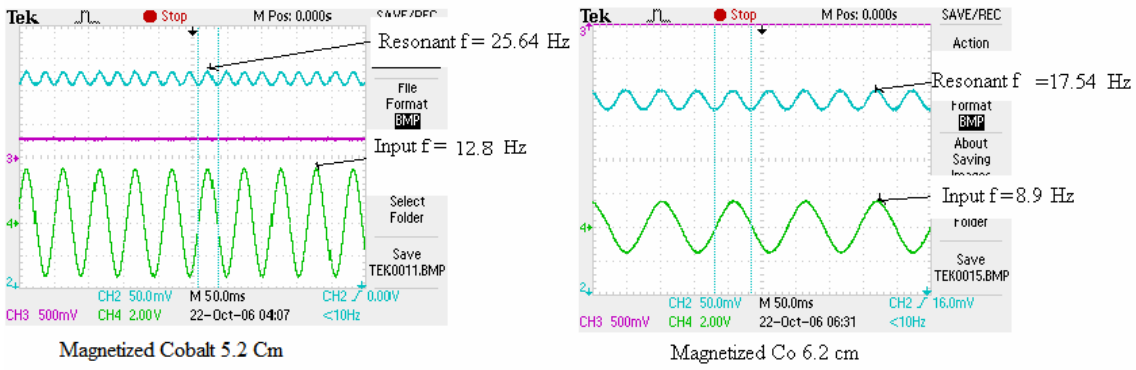

Figure 4.9: Input and output waveforms during dynamic measurements.

4.4.1 *Nickel Powder Coating*

The dynamic displacements are performed similarly like in chapter 3. The magnetized Nickel powder is used to perform the dynamic displacements of 4.2cm, 5.2cm, 6.2cm and 7.2cm fibers. The Fig. 4.10 shows the dynamic displacements and resonant frequencies of the Nickel coated fiber. Which is summarizes in table 4.3.

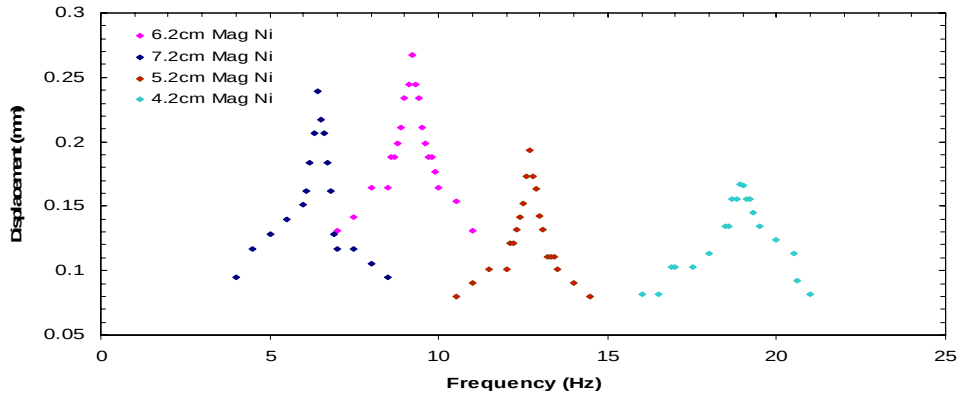

Figure 4.10: Dynamic displacements using Nickel powder coating.

Table 4.3: Comparison of Resonant Frequencies for Nickel Coated Fibers.

Lengths (Cm)	Calculated Resonant Frequencies (Hz)	Experimental Resonant Frequencies (Hz)
4.2	36.2	37.4
5.2	24.76	25
6.2	17.24	17.56
7.2	12.44	12.82

4.4.2 Iron Powder Coating

Similarly, the magnetized Iron powder was used to perform the dynamic displacements of 4.2cm, 5.2cm, 6.2cm and 7.2cm fibers. The Fig. 4.11 shows the dynamic displacements and resonant frequencies of the Nickel coated fibers. Which is summarizes in Table 4.4.

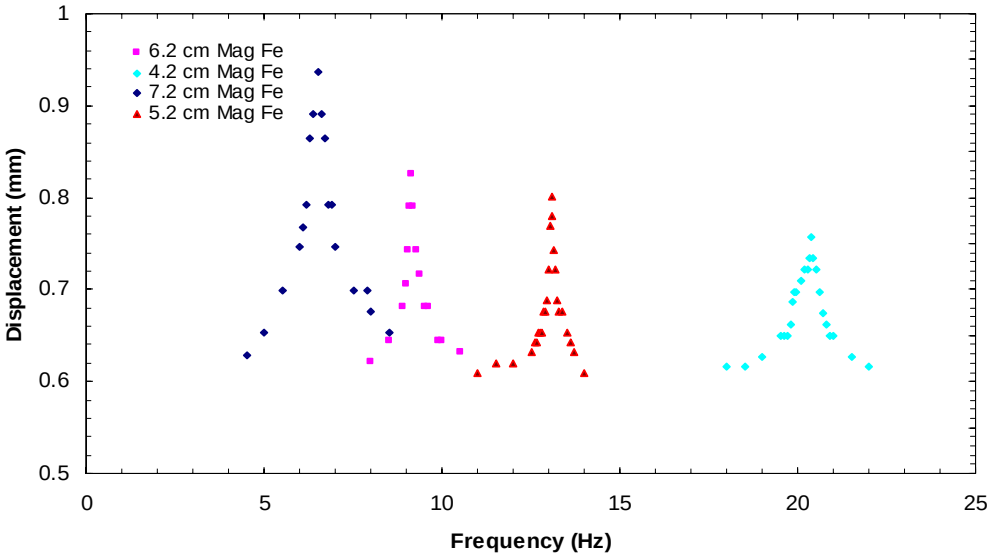

Figure 4.11: Dynamic displacements using Iron powder coating.

Table 4.4: Comparison of Resonant Frequencies for Iron Coated Fiber.

Lengths (Cm)	Calculated Resonant Frequencies (Hz)	Experimental Resonant Frequencies (Hz)
4.2	36.9	40.23
5.2	25.2	26.32
6.2	16.9	17.86
7.2	11.83	12.2

4.4.3 Cobalt Powder Coating

In the same way, the magnetized Iron powder was used to perform the dynamic

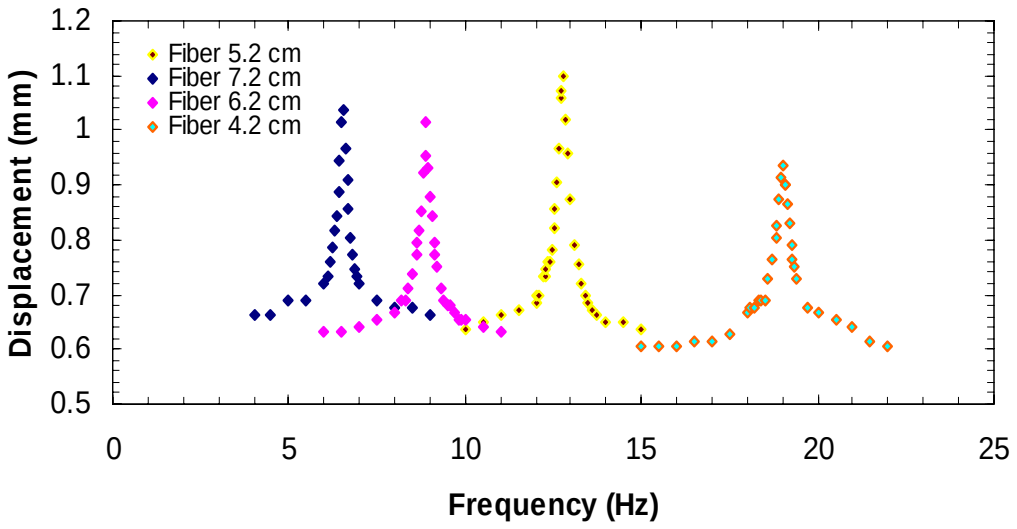

Figure 4.12: Dynamic displacements using Cobalt powder coating.

displacements of 4.2cm, 5.2cm, 6.2cm and 7.2cm fibers. The Fig. 4.12 shows the dynamic displacements and resonant frequencies of the Cobalt coated fiber. Which is summarizes in Table 4.5.

Table 4.5: Comparison of Resonant Frequencies for Cobalt Coated Fibers.

Lengths (Cm)	Calculated Resonant Frequencies (Hz)	Experimental Resonant Frequencies (Hz)
4.2	34.02	37.4
5.2	23.73	25
6.2	17.21	17.54
7.2	12.56	12.82

4.4.4 Comparison of the Dynamic Displacements of All Lengths

Likewise, all magnetized ferromagnetic materials have used to perform the dynamic displacements of different lengths of fibers. The Table 4.6 shows that the magnetized Cobalt has the highest actuation than magnetized Nickel and magnetized Iron.

Table 4.6: Comparison of Dynamic Displacements for Magnetized Materials.

Lengths (Cm)	Displacements using Iron Powder (mm)	Displacements using Cobalt Powder (mm)	Displacements using Nickel Powder (mm)
7.2	0.938	1.038	0.2339
6.2	0.825	1.014	0.267
5.2	0.801	1.098	0.343
4.2	0.757	0.9376	0.166

4.5 Theoretical and Experimental Displacements of Magnetized Cobalt Powder

From this chapter, it can be concluded that among the magnetized magnetic gels used in this experiment, magnetized Cobalt has the highest actuation. Thus, for the illustration, the theoretical values and experiment result for the magnetized Cobalt powder is shown in this section. The magnetization vector M is obtained similarly explained in section 3.4 by analyzing the measurement taken from AGM for the magnetized Cobalt powder. The theoretical static displacements were calculated in the same way as mentioned in section 3.4. Figure 4.13 shows the polynomial equation to calculate the magnetic vector movement using curve fitting method.

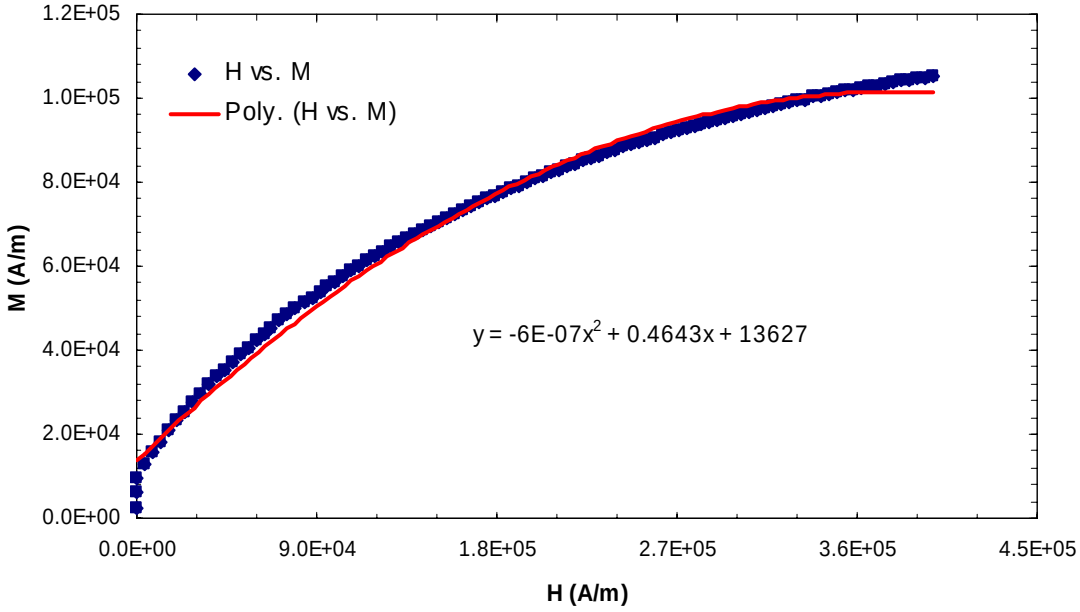

Figure 4.13: Polynomial equation of the magnetization vector.

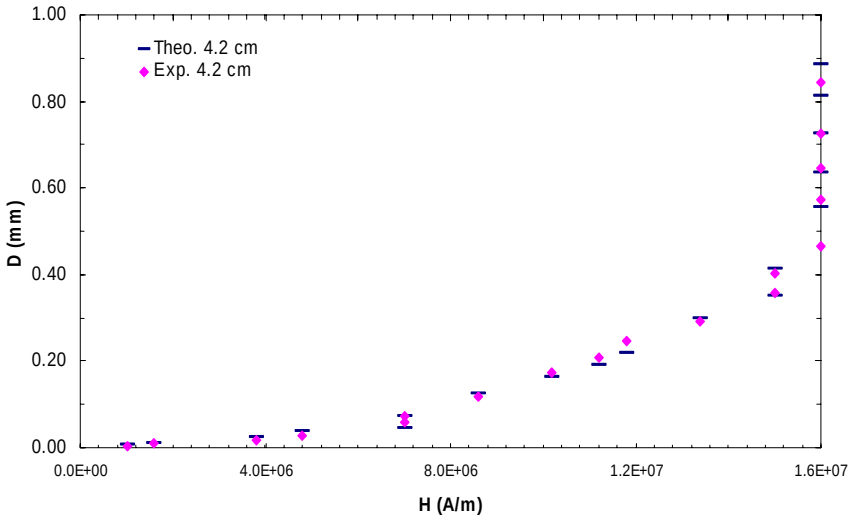

Figure 4.14: Theoretical vs. experimental static displacements for the 4.2cm fibers.

For length Fig. 4.14, the experimental displacements are higher in some values of input current than others. There could be various factors like the magnetization, thickness of the gel, radius of the gel etc for the inconsistent values.

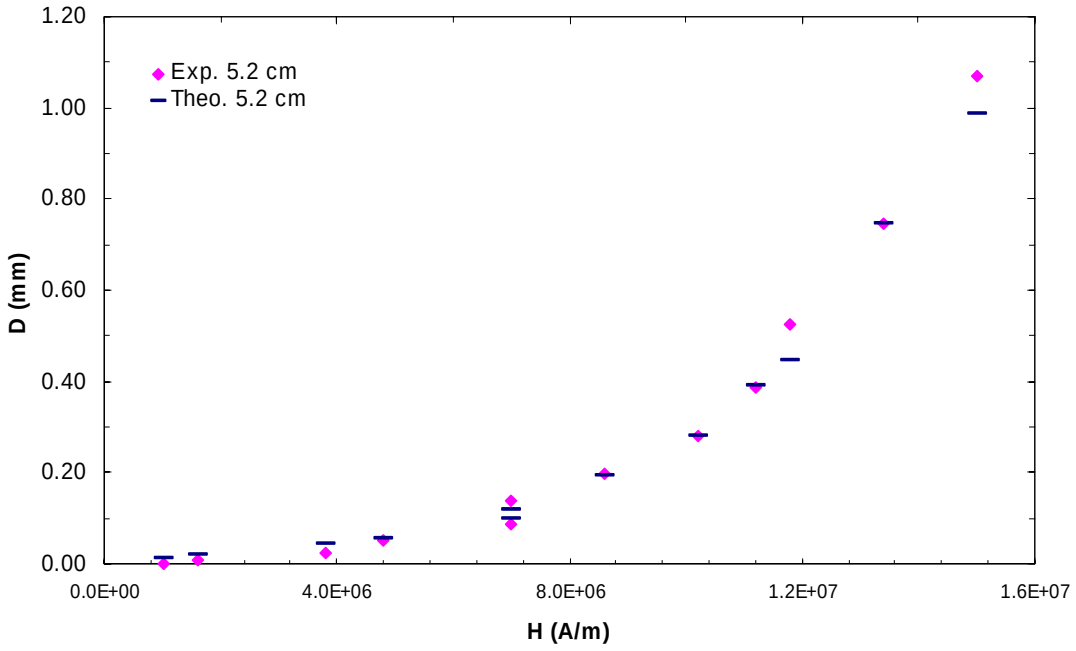

Figure 4.15: Theoretical vs. experimental static displacements for the 5.2cm fibers.

Being higher length, the 6.2cm has higher actuation than the length 5.2cm and 4.2cm. Figure 4.15 shows the theoretical and the experimental displacements of the 6.2cm magnetized cobalt coated fibers.

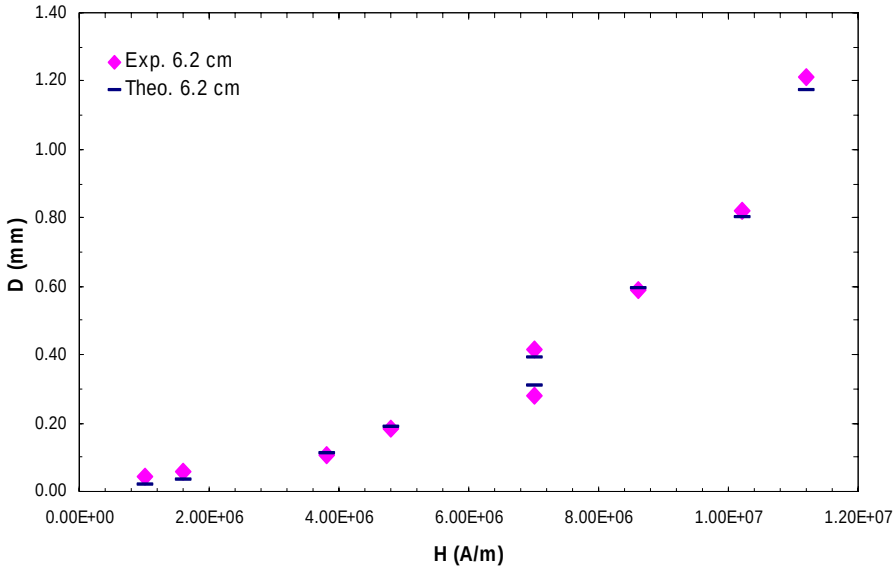

Figure 4.16: Theoretical vs. experimental static displacements for the 6.2cm fibers.

The length of 7.2cm has higher actuation than the length 6.2cm, 5.2cm and 4.2cm. Figure 4.15 shows the theoretical and the experimental displacements of the 6.2cm magnetized cobalt coated fibers. The theoretical and experimental displacements are similar in the lengths of 7.2cm and 6.2cm.

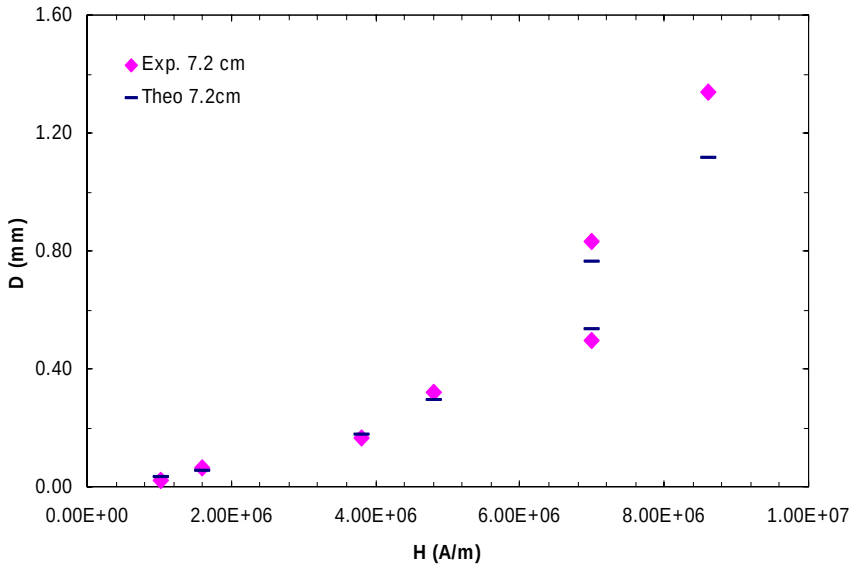

Figure 4.17: Theoretical vs. experimental static displacements for the 7.2cm fiber.

4.6 Conclusions

In short, the test for the magnetic characteristics of magnetized ferromagnetic materials was performed using AGM device and MicroMag software. The magnetic hysrersis curve and the other magnetic properties are found different for different magnetized ferromagnetic materials. Also the magnetized ferromagnetic materials have different magnetic properties than the non magnetized so the actuations of these materials are different than non magnetized. Among the magnetized materials, Cobalt has the highest displacements comparing to Nickel and Iron. The length 5.2 has the highest displacements 1.345 mm among other 7.2cm, 6.2cm 4.2cm while the input current is 260 mA. But in the point of view of powder consumption, 7.2cm fiber has the

highest displacements 1.338 mm among lengths 2.2cm, 3.2cm, 4.2cm, 5.2cm and 6.2cm while the input current is 120 mA. The electromagnet used during the experiment has only 201 kOe magnetic field intensity but the Samarium Cobalt powder has higher magnetic field intensity than the electromagnet. So, the actuation of the magnetized SmCo is negligible due to the weak electromagnet.

CHAPTER 5

RESULTS AND CONCLUSIONS

5.1 Results

From Chapters 3 and 4, it is concluded that cobalt has higher actuation than Nickel and Iron. Since the static displacements of magnetized cobalt powder has higher displacements than the non magnetized cobalt powder, it is proven from this experiment that the magnetized cobalt is better than non magnetized cobalt. As shown in Table 5.1, a length of 7.2cm has the highest displacements and it is suggested to choose in terms of power consumption.

Table 5.1: Static Displacements of Non Magnetized and Magnetized Cobalt Powder.

Lengths (Cm)	Current (mA)	Displacements using Cobalt Powder (mm)	Displacements using Magnetized Cobalt Powder (mm)
7.2	120	0.771	1.338
6.2	160	0.702	1.213
5.2	220	0.853	1.345
4.2	340	0.760	0.842

Likewise, from the Chapters 3 and 4, it is shown that dynamically cobalt has better actuation than Iron and Nickel. Also it is proven from this experiment that the magnetized cobalt has better actuation than non magnetized cobalt. Table 5.2 shows that length 5.2cm has highest displacements than other lengths but length 7.2cm has the highest displacements in terms of power consumption. The input voltage and input frequencies of 5.2cm fiber are 3 volt pick to pick and 12.5 Hz respectively but the input voltage and frequencies for 7.2cm fiber is 1 volt pick to pick and 6.5 Hz respectively.

Table 5.2: Dynamic Displacements of Non Magnetized and Magnetized Cobalt Powder.

Lengths (Cm)	Displacements using Cobalt Powder (mm)	Displacements using Magnetized Cobalt Powder (mm)
7.2	0.846	1.038
6.2	0.764	1.014
5.2	0.885	1.098
4.2	0.751	0.937

5.2 Conclusions

A fiber optic scanner was designed, fabricated and characterized as explained above. In this research, the silica optical fiber was chosen over the plastic optical fiber. Due to the low Young's modulus of the plastic optical fiber, the fiber bent during the

experiment due to its softness. Therefore, the silica optical fiber was used as the ultimate solution over the plastic optical fiber.

The spring constant also effects the actuation because the displacements are calculated by dividing the magnetic force by spring constant. So, higher spring constant lengths such as 2.2cm, and 3.2cm have low actuation than the lower spring constant lengths like 4.2cm, 5.2cm, 6.2cm and 7.2cm. Thus, the best length in terms of the power consumption is 7.2cm.

Therefore, the different ferromagnetic materials were used to characterize the fiber optic scanner. The magnetic properties of Cobalt, Iron, Nickel and Samarium Cobalt powders were measured before magnetization and after magnetization. These ferromagnetic materials have different characteristic before magnetization and after magnetization. The difference in magnetic properties was measured using Alternating Gradient Magnetometer (AGM) and MicroMag Model 2900 software. Among the magnetic properties of all four materials, Samarium Cobalt has the strongest magnetic property. Being one of the strongest earth's hard magnets, the magnetic field strength of the Samarium Cobalt was beyond the range of MicroMag.

Among the non magnetized materials, Cobalt has the highest displacements comparing to Nickel and Iron. The length 5.2 has the highest displacements among all other 7.2cm, 6.2cm 4.2cm while the input current is 260 mA. But in the point of view of powder consumption, 7.2cm fiber has the highest displacements among all lengths 2.2cm, 3.2cm, 4.2cm, 5.2cm and 6.2cm while the input current is 120 mA. The

electromagnet used during the experiment did not have higher magnetic field intensity to actuate Samarium Cobalt powder.

The magnetized ferromagnetic materials have different magnetic properties than the non-magnetized materials, subsequently the actuation of these materials are different than non magnetized. Among the magnetized materials, Cobalt has the highest displacements comparing to Nickel and Iron. The length 5.2 has the highest displacements among other 7.2cm, 6.2cm 4.2cm while the input current is 260 mA. Nevertheless, by the point of view of powder consumption, 7.2cm fiber has the highest displacements among all lengths 2.2cm, 3.2cm, 4.2cm, 5.2cm and 6.2cm while the input current is 120 mA. Despite that, the electromagnet used during the experiment did not have enough magnetic field intensity to actuate Samarium Cobalt powder.

Finally, it can be concluded that magnetized cobalt actuates better than cobalt providing the length 5.2cm of magnetized Cobalt as the ideal length for the best actuation in terms of the displacements. However, if it is chosen in terms of the power consumption, the length 7.2cm for magnetized cobalt can be the best alternate among all.

5.3 Future Work

The actuation of the 7.2cm and 5.2cm fibers using SmCo powder with high magnetic Field Strength Magnet can be considered as future work.

APPENDIX A

UNIT CONVERSION

Symbol	Quantity	Conversion from Gaussian and CGS EMU to SI [a]
H	Magnetic Field Strength	1 Oe $\rightarrow 10^3/(4\pi)$ A/m
m	Magnetic Moment	1 erg/G = 1 emu $\rightarrow 10^{-3}$ A·m^2 = 10^{-3} J/T
M	Magnetization Vector	1 erg/(G·cm^3) = 1 emu/cm^3 $\rightarrow 10^3$ A/m
μ	permeability	$1 \rightarrow 4\pi \times 10^{-7}$ H/m $= 4\pi \times 10^{-7}$ Wb/(A·m)

REFERENCES

1. S. P. Fang, and H. F. Taylor. “High-performance single-mode fiber-optic switch”, *Optics Letters*, 19:1204-1206. 1994.
2. Shi-Sheng Lee, Ed Motamedi, and Ming C. Wu. “Surface-micromachined free-Space Fiber Optic Switches With Integrated Microactuators for Optical Fiber Communication Systems”, *Transconductor’97 1997 International Conference on Solid-State Sensors and Actuators*, Chicago, June 16-19. 1997.
3. I. R. Matias, M. Lopez-Amo, F. Montero, C. Fernandez-Valdivielso, F. J. Arregui, and C. Bariain. “Low-cost optical amplitude modulator based on a tapered single-mode optical fiber”, *Applied Optics*, Vol. 40, No.2. January 2001.
4. S.A. Boppart, B.E. Bouma, C. Pitris, G.J. Tearney, and J.G. Fujimoto. “Forward-imaging instruments for optical coherence tomography”, *Optics Letters*, Vol. 22, No. 21. November 1997.
5. Nelson RW, Krone JR, and Jansson O. “Surface plasmon resonace biomolecular interaction analysis mass spectrometry”, *Anal Chem*, 69(21):4369-74. Nov 1997.
6. Miroslav Sedlar, Vlastimil Matejec, and Ivan Paulicka. “Optical fiber magnetic field sensors using ceramic magnetostrictive jackets”, *Sensors and Actuators*, 84: 297-302. 2000.

7. R.S. Popovic, J.A. Flanagan, and P.A. Besse. “The future of magnetic sensors”, *Sensor and Actuators*, A56:39-55. 1996.
8. Franz Keplinger, Samuel Kvasnica, Artur Jachimowicz, Franz Kohl, Johannes Steurer, and Hans Hauser. “Lorentz force based magnetic field sensor with optical readout”, *Sensors and Actuators*, A 110:112-118. 2004.
9. S.P. Fang and H.F. Taylor. “High-performance single-mode fiber-optic switch” *Optics Letters*, Vol. 19, No. 15. 1994.
10. Shi-Sheng Lee, Ed Motamedi, and Ming C. Wu. “Surface-micromachined free-space fiber optic switches with integrated microactuators for optical fiber communication systems”, *Transconductor’97 1997 International Conference on Solid-State Sensors and Actuators*, Chicago, June 16-19. 1997.
11. Mark Herding, Franz Richardt, and Peter Woias. “A novel approach to low-cost optical fiber switches”. *IEEE*. 2003.
12. Martin Hoffmann, Peter Kopka, Edgar Voges. „Bistable micromechanical fiber-optic switches on silicon with thermal actuators”, Sensors and Actuators, 78:28-35. 1999.
13. Kevin R. Cochran, Lawrence Fan, Don L. DeVoe. “High-power optical microswitch based on direct fiber Actuation”, *Sensor and Actuators*, October 2004.
14. Shinji Nagaoka. “Compact latching-type single-mode-fiber switches fabricated by a fiber-micromachining technique and their practical applications”, *IEEE*

Journal of Selected Topics in Quantum Electronics, Vol. 5, No. 1. January/February 1999.

15. Jonathan J. Bernstein, William P. Taylor, John D. Brazzle, Christopher J. Corcoran, Gregory Kirkos, Jefferson E. Odhner, Ajay Pareek, Marc Waelti, and Marvin Zai. "Electromagnetically actuated mirror arrays for use in 3-D optical swtiching applications", *Journal of Microelectromechanical Systems*, Vol. 13, No. 3. June 2004.
16. Merritt N. Deeter. "High sensitivity fiber-optic magnetic field sensors based on iron garnets", *IEEE Transactions on Instrumentation and Measurement*, Vol. 44, No. 2. April 1995.
17. G.J. Tearney, B.E. Bouma, S.A. Boppart, and B. Golubovic "Rapid Acquisition of in vivo Biological Images by Use of Optical Coherence Tomography," *Optics Letters*, VOL. 21, NO. 17, September 1,1996.
18. Naresh Dhaubanjar. "The Design And Analysis Of Optical Scanners For Optical Coherence Tomography", *UTA Thesis*, 2006.
19. http://usa.hamamatsu.com/assets/pdf/catsandguides/Psd.pdf
20. J. Topfer, and V. Christoph. "Multi-pole magnetization of NdFeB sintered magnets and thick films for magnetic micro-actuators" *Sensors and Actuators*, A113:257-263. 2004.
21. M. Sendoh, Ishiyama, and K.-I. Arai. "Fabrication of magnetic actuator for use in a capsule endoscope", *IEEE Transactions on Magnetics*, Vol. 39, No. 5. September 2003.

22. David Jiles. “Introduction to MAGNETISM and MAGNETIC MATERIALS”, *1st ed. Chapman and Hall*. P.75.

23. Kurt E. Petersen, “Dynamic Micromechanics on Silica: Techniques and Devices,” *IEEE Transactions on Electron Devices*, Vol. ED-25, No. 10, October 1978.

24. Http://scitation.aip.org/getpdf/servlet/GetPDFServlet?filetype=pdf&id=APPLAB000088000016163901000001&idtype=cvips&prog=normal

25. P. M. Hagelin, U. Krishnamoorthy, C. M. Arft, J. P. Heritage, and O. Solgaard, “Scalable fiber optic switch using micromachined mirrors,” *in Proc. 10th Int. Conf. Solid-State Sensors and Actuators (Transducers ’99)*, Sendai, Japan, June 7–10, 1999, 2P6-2.

26. M.-H. Kiang, O. Solgaard, K. Y. Lau, and R. Muller, “Polysilica optical microscanners for laser scanning displays,” *Sensors Actuators A70*, pp. 195-199, 1998.

27. R. A. Conant, P. M. Hagelin, U. Krishnamoorthy, and O. Solgaard, “A raster-scanning full-motion video display using polysilica micromachined mirrors,” *in Proc. 10th Int. Conf. on Solid-State Sensors and Actuators (Transducers ’99)*, Sendai, Japan, June 7–10, 1999, 2P3-2.

28. http://www3.interscience.wiley.com/cgi-bin/abstract/89016376/ABSTRACT?CRETRY=1&SRETRY=0

BIOGRAPHICAL INFORMATION

Pratibha Chaulagai Phuyal has been interested in Physics, Math and Material Science. She received her Bachelor of Science in Electrical Engineering degree in May 2003 from The University of Texas at Arlington, and Master of Science in Electrical Engineering degree in December 2006 from The University of Texas at Arlington. She has done research and Projects in MEMS, Bio-MEMS, CMOS RFIC, VLSI and CMOS Mix Signal IC. Her future goal is to achieve PhD Degree in one of her areas of interest.